PHYSICAL REVIEW B **96**, 214514 (2017)

Superconductivity in three-dimensional spin-orbit coupled semimetals

Lucile Savary,[1,2,*] Jonathan Ruhman,[1,†] Jörn W. F. Venderbos,[1] Liang Fu,[1] and Patrick A. Lee[1]

[1]*Department of Physics, Massachusetts Institute of Technology, 77 Massachusetts Ave., Cambridge, Massachusetts 02139, USA*

[2]*Université de Lyon, École Normale Supérieure de Lyon, CNRS, Université Claude Bernard Lyon I, Laboratoire de physique, 46, allée d'Italie, 69007 Lyon, France*

(Received 17 July 2017; revised manuscript received 4 December 2017; published 28 December 2017)

Motivated by the experimental detection of superconductivity in the low-carrier density half-Heusler compound YPtBi, we study the pairing instabilities of three-dimensional strongly spin-orbit coupled semimetals with a quadratic band touching point. In these semimetals the electronic structure at the Fermi energy is described by spin $j = \frac{3}{2}$ quasiparticles, which are fundamentally different from those in ordinary metals with spin $j = \frac{1}{2}$. For both local *and nonlocal* pairing channels in $j = \frac{3}{2}$ materials we develop a general approach to analyzing pairing instabilities, thereby providing the computational tools needed to investigate the physics of these systems beyond phenomenological considerations. Furthermore, applying our method to a generic density-density interaction, we establish that: (i) The pairing strengths in the different symmetry channels uniquely encode the $j = \frac{3}{2}$ nature of the Fermi surface band structure—a manifestation of the fundamental difference with ordinary metals. (ii) The leading odd-parity pairing instabilities are different for electron doping and hole doping. Finally, we argue that polar phonons, i.e., Coulomb interactions mediated by the long-ranged electric polarization of the optical phonon modes, provide a coupling strength large enough to account for a Kelvin-range transition temperature in the s-wave channel, and are likely to play an important role in the overall attraction in non-s-wave channels. Moreover, the explicit calculation of the coupling strengths allows us to conclude that the two largest non-s-wave contributions occur in *nonlocal* channels, in contrast with what has been commonly assumed.

DOI: 10.1103/PhysRevB.96.214514

I. INTRODUCTION

Increasingly many low density materials are being found to superconduct. Examples include a rather diverse set of two-dimensional (2D) and three-dimenbsional (3D) materials, doped topological insulators, semiconductors, and semimetals, such as $Cu_xBi_2Se_3$ [1], $Pb_{1-x}Tl_xTe$ [2], single crystal Bi [3], Bi-based half-Heusler compounds, e.g., YPtBi and ErPdBi [4], and of course doped $SrTiO_3$ has been known to superconduct for more than 50 years [5]. In addition to a low density of carriers, many of these materials share a number of other properties: sizable spin-orbit coupling, pointers to unconventional pairing, weak Coulomb repulsion due to a large dielectric screening, and in some cases "proximity" to a topological phase. In this context, questions which naturally arise are: What is the mechanism for such low-density superconductivity in those materials? Is it related to spin-orbit coupling? Is it particularly conducive to unconventional pairing?

Strong spin-orbit coupling causes the multiplicity of bands at high symmetry points in the Brillouin zone, such as the Γ point, to be larger than two, a signal that the bands themselves transform under a nontrivial/high-dimensional representation of the crystal symmetry group. As a result, several of these materials host quasiparticles with large spin, e.g., $j = \frac{3}{2}$ rather than the conventional $j = \frac{1}{2}$. In particular, four-band $j = \frac{3}{2}$ structures emerge from the Γ_8 states in cubic symmetry. They have been known for a long time [6–8], but have recently attracted considerable interest due to their relevance to the *strongly correlated* pyrochlore iridates where a flurry of unusual behaviors were uncovered [9–14]. Superconductivity, however, is absent in the iridates, where instead magnetic order develops at low temperature [15,16].

In this context, the Bi-based half-Heusler superconductors such as RPtBi and RPdBi, where R is either a rare-earth or Y/Lu, offer ideal ground for the study of low-density superconductivity in spin-orbit coupled systems and provide many potential examples of unconventional superconductors [4,17–26]. Indeed, these materials share a very similar band structure with the paramagnetic pyrochlore iridates, but exhibit superconductivity at low temperature rather than magnetic order. Most compounds in this family have a superconducting transition temperature close to 1 K, ranging from approximately 0.7 K in DyPdBi and 0.77 K in YPtBi, to 1.6 K in YPdBi. The density of carriers (due to accidental doping) has been estimated at 10^{18} cm^{-3} in the Pt family, and is roughly 10^{19} cm^{-3} for the Pd materials [4]. The Fermi energy intercepts two bands with $j = \frac{3}{2}$ character [27] close to where they meet (at the Γ point), and like in the pyrochlore iridates, *ab initio* calculations [26,28,29] and ARPES on YPtBi [26] show that (i) around the Γ point two bands lie above the touching point while two bands lie below it and (ii) pockets elsewhere in the Brillouin zone seem to be absent, at least in some of the compounds in the family (and hence the Fermi energy crosses only two bands). Most importantly, the predominantly Bi p-orbital character of the bands most likely produces only weak correlations, as is evident from a very large bandwidth, leaving only electronic and lattice (phonon) degrees of freedom as candidates for mediating superconductivity.

Superconductivity at very low densities presents two challenges for conventional BCS theory: First, the Fermi energy can become so low that it is smaller than the relevant phonon energy, implying that the usual renormalization of the Coulomb repulsion from $\mu = \langle V_C \rangle_{FS}$ (the Coulomb

*savary@mit.edu
†ruhman@mit.edu

interaction strength averaged over the Fermi surface) to μ^* is no longer applicable, as is the case for doped $SrTiO_3$ [30]. For the half-Heuslers, the Fermi energy is larger than the Debye frequency, but it is still of the same order [31]. Second, in 3D, the density of states at the Fermi energy $N(0)$ goes to zero as the carrier density is reduced. In standard BCS theory, $T_c \propto \exp\{-1/[N(0)V]\}$, where V is the pairing interaction strength. For metals, the electron-phonon interaction is well screened so that V is typically short ranged, and T_c is expected to be exponentially small as the density becomes small. This issue was discussed a long time ago in a seminal work by Gurevich, Larkin, and Firsov (GLF) [32], who concluded that for a *short-ranged* attractive interaction superconductivity was not expected at densities lower than $10^{19}\,\mathrm{cm}^{-3}$, in line with expectations. They proposed, however, that electron-phonon interactions could circumvent the problem of a low density of states and efficiently mediate superconductivity in ionic crystals where the lattice distortion caused by an optical phonon generates polarization (electric dipoles), and in turn effectively a *long-ranged* electron-phonon interaction. Such an interaction is captured by the Frölich Hamiltonian [33], and, being long ranged, benefits from lower densities where it is not as effectively screened by other electrons in the system. LDA calculations on YPtBi found the short-ranged electron-phonon $N(0)V$ to be 0.02 [28], much too small to support superconductivity, but the numerical package used to obtain this result did not capture the Frölich coupling [34], leaving open the possibility that the GLF mechanism be responsible for superconductivity in this material. This is what we investigate in this paper.

To study superconductivity in a spin-orbit coupled multi-orbital system such as YPtBi, it is crucial to fully account for the Γ_8 character of the electronic states at the Fermi energy. This was addressed in an important recent paper by Brydon *et al.* [29], who pointed out that pairing of these spin $j = \frac{3}{2}$ electrons was markedly different from pairing of ordinary $j = \frac{1}{2}$ electrons, whereas in the latter case only spin-singlet and spin-triplet pairing states can be formed, since $\frac{1}{2} \otimes \frac{1}{2} = 0 \oplus 1$, Cooper pairs composed of two $j = \frac{3}{2}$ electrons can have higher spin, following $\frac{3}{2} \otimes \frac{3}{2} = 0 \oplus 1 \oplus 2 \oplus 3$.

We will demonstrate that the nontrivial transformation of the bands also has important implications for the pairing instabilities, and is most clearly seen when projecting the pair scattering interaction onto the Fermi surface. Indeed, as mentioned above, the symmetry group of the crystal enforces the touching of all four bands at the Gamma point, but only requires twofold degeneracy away from it (by Kramers theorem through the existence of inversion and time-reversal symmetries). Spin-orbit coupling can then lead to a bending of the bands in opposite ways (see Fig. 1), so that the Fermi energy crosses just two degenerate bands with pseudospin index σ. Since only electronic states close to the Fermi surface contribute to pairing, the problem is superficially reminiscent of that with a spin-$\frac{1}{2}$ degree of freedom. However, the structure of the Fermi surface pseudospin states is very different, owing to the $j = \frac{3}{2}$ nature of the Γ_8 bands. The projection of the interactions onto the bands at the Fermi energy renders this fact evident as the structure of the spin-orbit coupled Γ_8 bands is reflected in the effective coupling constants obtained from

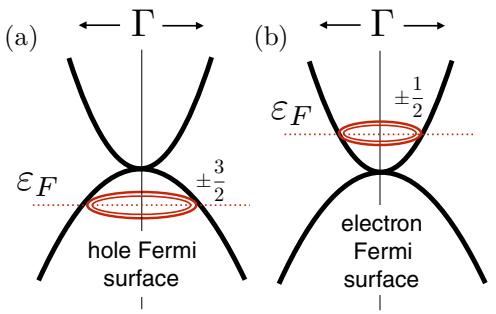

FIG. 1. (a) Schematic electronic band structure of quadratic band crossing semimetals such as YPtBi. The touching of the Γ_8 bands at the Gamma point is protected by symmetry. In the presence of strong spin-orbit coupling, i.e., coupling of the quasiparticle spin and crystal momentum, see Eqs. (3) and (4), and with inversion symmetry the Γ_8 bands are split into two twofold degenerate bands away from Γ. Motivated by YPtBi, we assume that one of these bands curves upward, forming the electron band, and one curves downward, forming the hole band. In YPtBi, when the Fermi energy is in the hole band, corresponding to hole doping, the quasiparticle states on the Fermi surface are spin $\pm\frac{3}{2}$ states, in the spherical approximation. (b) In the case of electron doping, which we also consider, the quasiparticle states on the Fermi surface are spin $\pm\frac{1}{2}$ states.

decomposing the projected interaction into irreducible pairing channels, which themselves govern the instabilities towards superconductivity.

This has deep implications for the pairing instabilities. For instance, we will demonstrate that the effective coupling constants of odd-parity pairing channels, which directly relate to T_c, are different for the hole and electron Fermi surfaces, even though their dispersions are similar.

In this paper we develop a general approach to studying pairing instabilities in doped spin-orbit coupled $j = \frac{3}{2}$ systems with quadratic band touching dispersion. We identify the relevant symmetry quantum numbers and decompose the pair scattering interaction into irreducible pairing channels, including nonlocal ones. This decomposition reveals the natural mean-field decouplings, which can be used to derive the corresponding BCS (or Eliashberg) gap equations. Many of the features specific to $j = 3/2$ systems become apparent when we project the interactions onto the bands at the Fermi surface. Our approach is independent of the symmetry group of the normal state, though we apply the formalism to the half-Heusler material YPtBi and for ease of presentation generally assume full spherical symmetry before discussing the effect of cubic crystal fields.

The remainder of the paper is organized as follows. We first provide the band structure model relevant to the half-Heuslers, and introduce the density-density interaction we will be considering throughout. We then turn to a classification and rewriting of the interaction into irreducible representation components, and consider the projection of these terms onto the valence bands. We finally derive the appropriate Eliashberg equations before moving on to a discussion of the results.

II. BAND STRUCTURE AND INTERACTIONS

We start our analysis by introducing the model appropriate to describe the low-energy electronic physics of nonmagnetic

half-Heuslers. The electronic action consists of two terms: a quadratic term, representing the free kinetic part, and a quartic term, describing the interactions. We write

$$\mathcal{S} = \mathcal{S}_0 + \mathcal{S}_{\rm int}. \tag{1}$$

In what follows we discuss each of these terms in detail.

A. Band Hamiltonian

The free quadratic part of the action is given by

$$\mathcal{S}_0 = \sum_{\mathbf{r}} \int d\tau \psi^\dagger_{\mathbf{r}\tau}[\partial_\tau + \mathcal{H}_0(-i\nabla)]\psi_{\mathbf{r}\tau}, \tag{2}$$

where $\psi^\dagger = (\psi^\dagger_{\frac{3}{2}}, \psi^\dagger_{\frac{1}{2}}, \psi^\dagger_{-\frac{1}{2}}, \psi^\dagger_{-\frac{3}{2}})$ is a four-component creation operator of spin $j = \frac{3}{2}$ fermions and [35]

$$\mathcal{H}_0(\mathbf{k}) = \alpha_1 \mathbf{k}^2 + \alpha_2(\mathbf{k}\cdot\mathbf{J})^2 + \alpha_3\left(k_x^2 J_x^2 + k_y^2 J_y^2 + k_z^2 J_z^2\right) + \alpha_4 \mathbf{k}\cdot\mathbf{T} - \mu. \tag{3}$$

In the first line, $\mathbf{J} = (J_x, J_y, J_z)$ are the three 4×4 spin matrices of $j = \frac{3}{2}$ electrons. In addition, μ is the chemical potential (such that $\mu > 0$, respectively, $\mu < 0$, corresponds to electron, respectively, hole doping) and $\alpha_{1,2,3,4}$ are material-dependent parameters characterizing the electronic band structure. When $\alpha_3 = \alpha_4 = 0$ the system has full spherical symmetry. The term proportional to α_3 reduces the symmetry to cubic crystal symmetry while $\mathbf{k}\cdot\mathbf{T}$, with $T_x = \{J_x, J_y^2 - J_z^2\}$ and $T_{y,z}$ given by cyclic permutations, is only allowed in an inversion symmetry broken tetrahedral crystal field.

The Hamiltonian of Eq. (3) can be usefully rewritten in terms of anticommuting Γ matrices (see Appendix A) and the five d-wave functions $d_a(\mathbf{k})$ quadratic in momentum. One obtains

$$\mathcal{H}_0(\mathbf{k}) = c_0\mathbf{k}^2 + c_1\sum_{a=1}^{3} d_a(\mathbf{k})\Gamma_a + c_2\sum_{a=4}^{5} d_a(\mathbf{k})\Gamma_a + c_3\mathbf{k}\cdot\mathbf{T} - \mu. \tag{4}$$

The coefficient c_0 measures the particle-hole asymmetry in the band structure, while $|c_1 - c_2|$ measures its cubic anisotropy: $c_1 = c_2$ corresponds to full spherical symmetry, whereas $c_1 \neq c_2$ implies a splitting of the five d wave into T_{2g} and E_g subsets. When $c_3 = 0$, the system has both time-reversal and inversion symmetry, mandating a twofold degeneracy at each momentum $\mathbf{k}$. In that case, a simple expression for the energy eigenvalues can be obtained and is given by $\mathsf{E}_\nu(\mathbf{k}) = c_0\mathbf{k}^2 + \nu E_{\mathbf{k}} - \mu$, where ν denotes the band and corresponds to $+1$ for electron bands and -1 for the hole ones, and $E_{\mathbf{k}} = (c_1^2\sum_{a=1}^{3} d_a^2 + c_2^2\sum_{a=4}^{5} d_a^2)^{1/2}$. The Kramers degeneracy is labeled by the index σ. Thus, overall the Bloch states are denoted by $|\mathbf{k},\nu,\sigma\rangle$.

The condition $|c_0| \leqslant |c_1|/\sqrt{6}$ guarantees that two bands always curve upwards, forming the conduction band, while the other two curve downwards (see Fig. 1). In the presence of full spherical symmetry (i.e., $\alpha_3 = \alpha_4 = 0$ or $c_1 = c_2$ and $c_3 = 0$), $\mathbf{k}\cdot\mathbf{J}$ commutes with the Hamiltonian, as may be seen directly from Eq. (3), and so the projection of the spin along $\hat{\mathbf{k}}$ is a good quantum number. In other words, the quantization axis of the spin is locked to $\mathbf{k}$. The hole and electron bands in that case may be labeled according to 3/2 or 1/2, following $\nu\,\mathrm{sgn}(c_1)$: the band with $\nu\,\mathrm{sgn}c_1 = 1$ is the 3/2 band while that with $\nu\,\mathrm{sgn}c_1 = -1$ is 1/2. For the parameters of YPtBi [29] the hole $\nu = -1$ (electron $\nu = +1$) band is the pair with a projected moment of $\pm\frac{3}{2}$ ($\frac{1}{2}$). It is important to note that even though the electron and hole bands appear to have a similar dispersion (i.e., both look like quadratic bands, curving downward and upward, respectively), their structure, as encoded in the eigenstates, is inherently different. For example, one has $\langle \mathbf{k},\frac{3}{2},\sigma|\tilde{J}^+_{\mathbf{k}}|\mathbf{k},\frac{3}{2},-\sigma\rangle = 0$, while $\langle \mathbf{k},\frac{1}{2},\sigma|\tilde{J}^+_{\mathbf{k}}|\mathbf{k},\frac{1}{2},-\sigma\rangle \neq 0$, where $\tilde{J}^\pm_{\mathbf{k}}$ are the raising and lowering operators corresponding to $\tilde{J}^z_{\mathbf{k}} = \mathbf{J}\cdot\hat{\mathbf{k}}$.

While the half-Heusler compounds—space group $F\bar{4}3m$—actually lack inversion symmetry, *ab initio* calculations suggest that inversion breaking has only a weak effect on the band structure [8] as compared, e.g., to the cubic $Fd\bar{3}m$ in the pyrochlore iridates. Since the consequences of spin-orbit coupling seem to be most important, we expect that many of the notable results we derive hold in a similar form in the absence of inversion symmetry. Therefore, in the bulk of the paper we neglect the effects of the absence of inversion symmetry—namely we set $c_3 = 0$, $\alpha_4 = 0$, eliminating the terms linear in $\mathbf{k}$ in the band Hamiltonian. This allows us to carry out analytical calculations which in turn help provide a deeper understanding of the problem, and are also directly relevant to cubic materials with inversion symmetry.

B. Interactions

As explained, we focus here on the attractive interaction mediated by optical phonons through the Frölich electron-phonon coupling. The interaction term in Eq. (3) is part of the long-ranged Coulomb (density-density) interaction. Collecting position and imaginary time variables in the index $x = (\mathbf{r},\tau)$, the interaction takes the form

$$\mathcal{S}_{\rm int} = \frac{1}{2}\int_{x,x'} V(x-x')\psi^\dagger_x\psi_x\psi^\dagger_{x'}\psi_{x'}, \tag{5}$$

where $\int_x = \sum_{\mathbf{r}}\int d\tau$ and the interaction $V = V(\mathbf{r},\tau)$ has Fourier and Matsubara components

$$V(\mathbf{q},\omega) = \frac{4\pi e^2}{\varepsilon(\mathbf{q},\omega)q^2}. \tag{6}$$

The total dielectric function has three contributions

$$\varepsilon(\mathbf{q},\omega) = \varepsilon_\infty + \varepsilon_c(\mathbf{q},\omega) + \varepsilon_e(\mathbf{q},\omega). \tag{7}$$

ε_∞ comes from interband transitions, and

$$\varepsilon_c(\mathbf{q},\omega) = \frac{\varepsilon_0 - \varepsilon_\infty}{1 + [\omega/\omega_T(\mathbf{q})]^2} \tag{8}$$

is the polarization in *Matsubara* frequency due to a polar phonon mode. Note that for simplicity, we have considered the case of a single phonon mode. ω_T is the frequency of the transverse optical mode, which is related to the longitudinal one through the Lyddane-Sachs-Teller (LST) relation $\omega_L = \sqrt{\varepsilon_0/\varepsilon_\infty}\,\omega_T$. Finally, the last term ε_e is the electronic

polarization, taken within the random-phase-approximation (RPA) to be

$$\varepsilon_e(\mathbf{q},\omega) = -\frac{4\pi e^2}{q^2}\Pi_e(\mathbf{q},\omega), \tag{9}$$

where Π_e is the electronic polarization, which we will later take in the Thomas-Fermi approximation, where $4\pi e^2\Pi_e$ is replaced by $-q_{\mathrm{TF}}^2$. We leave the study of the full polarization function, which includes the non-Fermi liquid $V(q) \propto 1/q$ regime of the undoped quadratic band touching system [10,36], and plasmons, to a future publication. We expect that the plasmonic contribution, which introduces more complex momentum dependence in the interaction, will favor non-s-wave pairings.

III. IRREDUCIBLE PAIRING CHANNELS

The next step in our analysis is to obtain and classify the set of irreducible pairing channels. To this end, we rewrite the density-density interaction Eq. (5) as a pair scattering Hamiltonian and then decompose the pair scattering terms into irreducible scattering vertices. Pairing channels are labeled by the quantum numbers of the Cooper pairs, and this labeling applies to irreducible scattering vertices as well. The symmetry quantum numbers of the Cooper pairs clearly depend on the symmetry group of the system. In the presence of full rotational symmetry (i.e., ignoring cubic anisotropy), the Cooper pair quantum numbers are given by its "spin" angular momentum S, which corresponds to the band index, its orbital angular momentum L, which corresponds to the momentum dependence of the pairing function, and its total angular momentum $J = L + S$ (not be confused with the spin operators $J_{x,y,z}$). For ease of presentation and clarity we will present all derivations in the language of spherical symmetry, and later indicate what the modifications are in lower symmetry.

In the present case of $j = \frac{3}{2}$ fermions, the spin angular momentum of the Cooper pair can take the values $S = 0,1,2,3$ [37,38]. It is instructive to compare this to the more familiar case of spin $j = \frac{1}{2}$ fermions, which can form Cooper pairs of $S = 0$ (singlet) or $S = 1$ (triplet). In this case, a two-body density-density interaction can be decomposed into singlet and triplet scattering vertices. More precisely, if $c_{\mathbf{k}}^\dagger = (c_{\mathbf{k}\uparrow}^\dagger, c_{\mathbf{k}\downarrow}^\dagger)$ are the creation operators of spin-$\frac{1}{2}$ fermions, then one has the identity

$$\begin{aligned}(c_{\mathbf{k}}^\dagger c_{\mathbf{k}'})(c_{-\mathbf{k}}^\dagger c_{-\mathbf{k}'}) = {}& \tfrac{1}{2}[c_{\mathbf{k}}^\dagger i\sigma^y (c_{-\mathbf{k}}^\dagger)^T][(i\sigma^y c_{-\mathbf{k}'})^T c_{\mathbf{k}'}] \\ & + \tfrac{1}{2}[c_{\mathbf{k}}^\dagger \boldsymbol{\sigma} i\sigma^y (c_{-\mathbf{k}}^\dagger)^T]\cdot[(i\sigma^y c_{-\mathbf{k}'})^T \boldsymbol{\sigma} c_{\mathbf{k}'}],\end{aligned} \tag{10}$$

where the dot product is between components of $\boldsymbol{\sigma}$, i.e., $[c_{\mathbf{k}}^\dagger \boldsymbol{\sigma} i\sigma^y (c_{-\mathbf{k}}^\dagger)^T]\cdot[(i\sigma^y c_{-\mathbf{k}'})^T \boldsymbol{\sigma} c_{\mathbf{k}'}] \equiv \sum_\alpha [c_{\mathbf{k}}^\dagger \sigma^\alpha i\sigma^y (c_{-\mathbf{k}}^\dagger)^T][(i\sigma^y c_{-\mathbf{k}'})^T \sigma^\alpha c_{\mathbf{k}'}]$. The appearance of $i\sigma^y$ guarantees the symmetry and antisymmetry of the spin part of the Cooper pair wave function for triplet and singlet pairing because $i\sigma^y$ relates the fundamental and adjoint representations of SU(2), such that $i\sigma^y (c_{-\mathbf{k}}^\dagger)^T$ transforms as $c_{\mathbf{k}}$. Note that $i\sigma^y$ is antisymmetric, $(i\sigma^y)^T = -i\sigma^y$, and together with conjugation acts as a time-reversal operation on spin: $(-i\sigma^y)\boldsymbol{\sigma}^* i\sigma^y = -\boldsymbol{\sigma}$.

TABLE I. List of spin pairing matrices $\vec{M}_S$ introduced in Eq. (12). Quasiparticles with $j = \frac{3}{2}$ can form Cooper pairs with spin $S = 0,1,2,3$; a Cooper pair of spin S is created by the operator $\psi_{\mathbf{k}}^\dagger \vec{M}_S \gamma (\psi_{-\mathbf{k}}^\dagger)^T$. Fermi statistics requires that the overall pairing function is even. Thus, the pairing matrices with S even are allowed locally (i.e., momentum independent). On the other hand the odd matrices here must be further multiplied by an odd power of momentum, which leads to a richer classification. In Table II we present the resulting representations in the case of a a single power of momentum. Note that in cubic symmetry the SO(3) representations labeled by S are split into cubic representations labeled by R.

S	Even/odd	R	$\vec{M}_R$
0	Even	A_{1g}	I_4
2	Even	E_g	(Γ_4,Γ_5)
		T_{2g}	$(\Gamma_1,\Gamma_2,\Gamma_3)$
1	Odd	T_{1g}	$\frac{2}{\sqrt{5}}(J_x,J_y,J_z)$
3	Odd	A_{2g}	$\frac{2}{\sqrt{3}}(J_xJ_yJ_z + J_zJ_yJ_x)$
		T_{1g}	$\frac{-41}{6\sqrt{5}}(J_x,J_y,J_z) + \frac{2\sqrt{5}}{3}(J_x^3,J_y^3,J_z^3)$
		T_{2g}	$\frac{1}{\sqrt{3}}(T_x,T_y,T_z)$

In a manner fully analogous to Eq. (10), the interaction of Eq. (5), which describes two-body density-density interactions of spin-$\frac{3}{2}$ fermions, can be decomposed into irreducible spin channels labeled by $S = 0,1,2,3$. In this decomposition we make use of the antisymmetric matrix γ, which serves as the analog of $i\sigma^y$. In particular, γ satisfies $\gamma^T = -\gamma$ and $\gamma^T \mathbf{J}^* \gamma = -\mathbf{J}$, and it relates the fundamental and adjoint representations of spin-$\frac{3}{2}$ fermions: $\gamma(\psi^\dagger)^T$ transforms as ψ under rotations. In the usual basis of 3/2 eigenstates, the matrix γ is given explicitly by

$$\gamma = \begin{pmatrix} 0 & 0 & 0 & 1 \\ 0 & 0 & -1 & 0 \\ 0 & 1 & 0 & 0 \\ -1 & 0 & 0 & 0 \end{pmatrix}. \tag{11}$$

Now, taking the Fourier transform of Eq. (5) and going to Matsubara frequency space, the density-density product of operators can be decomposed into pair scattering terms as (suppressing the frequency index of the operators)

$$\begin{aligned}&(\psi_{\mathbf{k}}^\dagger \psi_{\mathbf{k}'})(\psi_{-\mathbf{k}}^\dagger \psi_{-\mathbf{k}'}) \\ &\quad = \frac{1}{4}\sum_S \psi_{\mathbf{k}}^\dagger \vec{M}_S \gamma (\psi_{-\mathbf{k}}^\dagger)^T \cdot (\psi_{-\mathbf{k}'})^T \gamma^T \vec{M}_S^\dagger \psi_{\mathbf{k}'},\end{aligned} \tag{12}$$

where the sum is over irreducible spin channels $S = 0,1,2,3$. The matrices $\vec{M}_S$ are 4×4 matrices such that $\psi_{\mathbf{k}}^\dagger M_S^\alpha \gamma (\psi_{-\mathbf{k}}^\dagger)^T$ creates a Cooper pair with total spin S. There are $2S + 1$ matrices collected in the vector $\vec{M}_S$, corresponding to the degeneracy of the channel S. The matrices $\vec{M}_S$ are normalized such that each component of the vector M_S^α satisfies $\mathrm{Tr}[M_S^\alpha (M_S^\alpha)^\dagger] = 4$ (no implicit summation over α). They are listed in Table I. For instance, in case of $S = 0$ the single matrix $M_{S=0}$ is simply equal to the identity; for $S = 1$ one has $\vec{M}_{S=1} \propto (J_x, J_y, J_z)$. We note in passing that since the $S = 0$ and $S = 1$ channels are commonly referred to as spin-singlet and spin-triplet, the $S = 2$ and $S = 3$ channels are sometimes referred to as

spin-quintet and spin-septet (e.g., in Refs. [26,29]). For the $L > 0$ channels this is unrelated to the actual multiplicity of the Cooper pair pairing channels, which is determined by J (and not S) and equal to $2J + 1$.

We note that the decomposition Eq. (12) can be viewed as a Fierz identity, as can Eq. (10) (see Appendix C). Furthermore, at this stage it is worth pointing out that the $S = 0$ channels in Eqs. (12) and (10), which are associated with s-wave pairing, have different numerical prefactors: $1/4$ and $1/2$, respectively. In fact, the numerical prefactors in Eqs. (12) and (10) are equal to $1/(2j + 1)$ and simply follow from the Fierz identities. Below we will find that these prefactors are important for the effective coupling constants in the s-wave channel.

We have now arrived at an expression for the interaction Eq. (5) of the following form, considering only zero linear momentum Cooper pairs

$$\mathcal{S}_{\rm int} = \frac{1}{8\beta\mathcal{V}} \sum_{k,k'} V(k-k') \times \sum_{S} \psi_k^\dagger \vec{M}_S \gamma (\psi_{-k}^\dagger)^T \cdot (\psi_{-k'})^T \gamma^T \vec{M}_S^\dagger \psi_{k'}, \quad (13)$$

where $\mathcal{V}$ is the total volume, β is the inverse temperature $\beta = 1/(k_{\rm B}T)$, and we have collected the momentum $\mathbf{k}$ and fermionic Matsubara frequencies ω in $k = (\mathbf{k},\omega)$.

To proceed with the derivation of irreducible pairing channels, we now focus on the orbital angular momentum of the Cooper pairs. The orbital angular momentum can be labeled by the quantum numbers L and $\mathcal{M}_L$, where $\mathcal{M}_L$ is the familiar $(2L + 1)$-fold degenerate magnetic quantum number, and the orbital part of the Cooper pair wave function is given by the spherical harmonics $Y_{L\mathcal{M}_L}(\hat{\mathbf{k}})$. Fermi statistics requires that L is even (odd) when S is even (odd).

The irreducible pairing channels are classified by the total angular momentum $J = L + S$ of the Cooper pairs. Using the rules of composition of angular momentum, we take the spherical harmonics $Y_{L\mathcal{M}_L}(\hat{\mathbf{k}})$ and spin matrices $\vec{M}_S$, and construct the spin-orbit coupled matrices $\vec{N}_J(\hat{\mathbf{k}})$ such that $\psi_{\mathbf{k}}^\dagger N_J^\alpha(\hat{\mathbf{k}}) \gamma (\psi_{-\mathbf{k}}^\dagger)^T$ creates a Cooper pair with total angular momentum J. The dimension of the vector $\vec{N}_J$ is $2J + 1$ and can be labeled by the index $\mathcal{M}_J$.

Let us take the case $L = 1$ as an example. Then, Fermi statistics restricts S to be odd: $S = 1,3$. The combination $(L,S) = (1,1)$ gives rise to the multiplets $J = 0,1,2$; from $(L,S) = (1,3)$ one finds $J = 2,3,4$. Then, using the p-wave spherical harmonics $Y_{1\mathcal{M}_1}(\hat{\mathbf{k}}) \sim \hat{\mathbf{k}}$ and the odd channels of the pair scattering interaction of Eq. (12), we obtain the irreducible pair scattering vertices labeled by J as

$$\hat{\mathbf{k}}\cdot\hat{\mathbf{k}}' \sum_{S=1,3} \psi_k^\dagger \vec{M}_S \gamma (\psi_{-k}^\dagger)^T \cdot (\psi_{-k'})^T \gamma^T \vec{M}_S^\dagger \psi_{k'} = \frac{1}{3} \sum_J \psi_k^\dagger \vec{N}_J(\hat{\mathbf{k}}) \gamma (\psi_{-k}^\dagger)^T \cdot (\psi_{-k'})^T \gamma^T \vec{N}_J^\dagger(\hat{\mathbf{k}}) \psi_{k'}, \quad (14)$$

where the sum over J is here a short-hand notation for a sum over the odd-S combinations $(L,S) = (1,1)$ $(J = 0,1,2)$ and $(L,S) = (1,3)$ $(J = 2,3,4)$, and the matrices $\vec{N}_J(\hat{\mathbf{k}})$ are normalized according to $\frac{1}{4\pi}\int d\hat{\mathbf{k}} {\rm Tr}[N_J^\alpha(\hat{\mathbf{k}}) N_J^{\alpha\dagger}(\hat{\mathbf{k}})] = 4$ (no implicit α summation). We list the matrices $\vec{N}_J(\hat{\mathbf{k}})$ in cubic representations in Table II. Note that $\sum_{\mathcal{M}_1} Y^*_{1\mathcal{M}_1}(\hat{\mathbf{k}}) Y_{1\mathcal{M}_1}(\hat{\mathbf{k}}') = 3\hat{\mathbf{k}}\cdot\hat{\mathbf{k}}'/4\pi$.

TABLE II. List of odd-parity total angular momentum pairing matrices $N_J(\mathbf{k})$ in cubic symmetry with inversion O_h constructed from the odd matrices in Table I and a factor of k^μ. A Cooper pair with total angular momentum J is created by one of the operators $\psi_{\mathbf{k}}^\dagger \vec{N}_J(\mathbf{k}) \gamma (\psi_{-\mathbf{k}}^\dagger)^T$. We defined $\mathcal{J} = \frac{-41}{6\sqrt{5}}\mathbf{J} + \frac{2\sqrt{5}}{3}(J_x^3, J_y^3, J_z^3)$. The additional horizontal space separates $S = 1$ (T_{1g}) from $S = 3$ $(A_{1g} + T_{1g} + T_{2g})$ channels.

R'	$\vec{N}_{R'}(\mathbf{k})$
A_{1u}	$\frac{2}{\sqrt{5}}\mathbf{k}\cdot\mathbf{J}$
T_{1u}	$\frac{\sqrt{6}}{\sqrt{5}}\mathbf{J}\times\mathbf{k}$
E_u	$\frac{\sqrt{2}}{\sqrt{5}}[-J_xk_x - J_yk_y + 2J_zk_z, \sqrt{3}(J_xk_x - J_yk_y)]$
T_{2u}	$\frac{\sqrt{6}}{\sqrt{5}}(J_yk_z + J_zk_y, J_xk_z + J_zk_x, J_xk_y + J_yk_x)$
T_{2u}	$-2\Gamma_{45}\mathbf{k}$
A_{1u}	$\mathcal{J}\cdot\mathbf{k}$
E_u	$\frac{1}{\sqrt{2}}[-k_x\mathcal{J}_x - k_y\mathcal{J}_y + 2k_z\mathcal{J}_z, \sqrt{3}(k_x\mathcal{J}_x - k_y\mathcal{J}_y)]$
T_{1u}	$\frac{\sqrt{3}}{\sqrt{2}}\mathcal{J}\times\mathbf{k}$
T_{2u}	$\frac{\sqrt{3}}{\sqrt{2}}(\mathcal{J}_yk_z + \mathcal{J}_zk_y, \mathcal{J}_xk_z + \mathcal{J}_zk_x, \mathcal{J}_xk_y + \mathcal{J}_yk_x)$
A_{2u}	$\frac{1}{\sqrt{3}}\mathbf{T}\cdot\mathbf{k}$
E_u	$\frac{1}{\sqrt{6}}[T_xk_x + T_yk_y - 2T_zk_z, \sqrt{3}(T_xk_x - T_yk_y)]$
T_{1u}	$\frac{1}{\sqrt{2}}(T_yk_z + T_zk_y, T_xk_z + T_zk_x, T_xk_y + T_yk_x)$
T_{2u}	$\frac{1}{\sqrt{2}}\mathbf{T}\times\mathbf{k}$

Equation (14) allows us to fully decompose the density-density interaction $V(\mathbf{q},\omega)$ into irreducible pairing vertices. In the presence of full rotational symmetry, the interaction can be expanded as a sum over products of spherical harmonics. Here and in the remainder of this paper we shall restrict the expansion to linear p-wave order in $\mathbf{k}$, i.e., to the order $L = 1$, and write

$$V(\mathbf{k}-\mathbf{k}',\omega-\omega') = V_0(\omega-\omega') + 3V_1(\omega-\omega')\mathbf{k}\cdot\mathbf{k}' + \cdots. \quad (15)$$

(see Appendix D) Note that the interaction parameters $V_{0,1,\ldots}$ can still depend on the magnitude of $\mathbf{k},\mathbf{k}'$; this is suppressed as it does not affect the rest of the analysis (and later we will take $|\mathbf{k}| = |\mathbf{k}'| = k_{\rm F}$). We then arrive at the final form of the interaction term given by

$$\mathcal{S}_{\rm int} = \frac{1}{8\beta\mathcal{V}} \sum_{k,k'} \sum_J \hat{V}^J_{\alpha\beta\gamma\delta}(\mathbf{k},\mathbf{k}';\omega-\omega') \psi^\dagger_{k\alpha} \psi^\dagger_{-k\beta} \psi_{-k'\gamma} \psi_{k'\delta}, \quad (16)$$

where here the sum over J runs over both the even and odd representations, i.e., the combinations $(L,S) = (0,0)$ $(J = 0)$, $(L,S) = (0,2)$ $(J = 2)$, and $(L,S) = (1,1)$ $(J = 0,1,2)$ and $(L,S) = (1,3)$ $(J = 2,3,4)$, and the spin-dependent pair scattering vertices $\hat{V}^J_{\alpha\beta\gamma\delta}$ take the form

$$\hat{V}^J_{\alpha\beta\gamma\delta} = \begin{cases} V_0[\vec{M}_J\gamma]_{\alpha\beta}\cdot[\gamma^T\vec{M}_J^\dagger]_{\gamma\delta} & \text{for } S = \text{even}, \\ V_1[\vec{N}_J(\mathbf{k})\gamma]_{\alpha\beta}\cdot[\gamma^T\vec{N}_J^\dagger(\mathbf{k}')]_{\gamma\delta} & \text{for } S = \text{odd}. \end{cases} \quad (17)$$

Here we have used that $\vec{N}_J(\mathbf{k}) = \vec{M}_J$ whenever S is even, since $L = 0$ in this case.

Up to this point in this section, we have particularized to the case of full spherical symmetry, which allowed us to label the irreducible pairing channels by symmetry quantum number J. In a cubic crystal, however, pairing channels are labeled by the representations of the cubic point group. Importantly, the decomposition schemes of Eqs. (13) and (16) remain valid [because Eqs. (12), (14), and (15) do], but the sums over the symmetry quantum numbers S, L, and J, all of which are labels of SO(3) representations, must be replaced by sums over cubic representations R. The effect of lower symmetry, i.e., cubic instead of full spherical symmetry, is to lift some of the degeneracies of the $J > 1$ channels. For instance, in a cubic environment the even-parity $L = 0$ channels acquire the symmetry labels

$$J = 0 \to A_{1g}, \quad J = 2 \to E_g + T_{2g}, \tag{18}$$

whereas the odd-parity pairing channels become

$$\begin{aligned} &J = 0 \to A_{1u}, \quad J = 1 \to T_{1u}, \quad J = 2 \to E_u + T_{2u}, \\ &J = 3 \to A_{2u} + T_{1u} + T_{2u}, \\ &J = 4 \to A_{1u} + E_u + T_{1u} + T_{2u}. \end{aligned} \tag{19}$$

In Table I we have listed the cubic symmetry labels of the spin matrices $\vec{M}_S$ and in Table II those for the odd S total angular momentum matrices $\vec{N}_J$. [Correspondence to the representations of the point group T_d of the half-Heuslers is provided in the Appendix B and Tables VI and VII.]

An important property of discrete crystal point groups is that the number of irreducible representations is finite. As a consequence, distinct pairing channels labeled by different J in full spherical symmetry may contain several copies of the same cubic representation, which implies that mixing is possible. This is exemplified by Eq. (19), from which we see that, e.g., certain $J = 1,3,4$ pairing matrices can mix with one another since all contain a representation with T_{1u} symmetry.

IV. PROJECTION ONTO THE VALENCE BANDS

As a preparatory step towards the derivation of the Eliashberg equation we now describe the process of projection to the states close to the Fermi energy. Since the electronic states relevant for the pairing instability are these states, it is natural to ignore pair scattering contributions which involve excitations at a higher energy scale, away from the Fermi surface. Usually this is a trivial step where completely empty or completely filled bands are ignored without any consequence. However, in the present case, where spin-orbit coupling is so strong that it splits the fourfold multiplet in a way that one pair of bands folds upwards and the other downwards the projection will have an important effect.

The chemical potential, in this case, either crosses the holelike valence band ($\nu = -1$) or the electronlike conduction band ($\nu = +1$). In the case of hole-doping applicable to YPtBi, we then project out the conduction band degrees of freedom and retain only the valence band pair scattering terms of the interaction V. To this end, we transform to the band basis and define the two-component valence band electron operators $c_{\mathbf{k}}$, which annihilate electrons in the eigenstates $|\mathbf{k},\nu = -,\sigma\rangle$. The operators $c_{\mathbf{k}}$ are related to the electron operators $\psi_{\mathbf{k}}$ by

$$c_{\mathbf{k}} = U_{\mathbf{k}}^{\dagger}\psi_{\mathbf{k}}, \tag{20}$$

where $U_{\mathbf{k}}$ is the 4×2 matrix of valence band eigenvectors (note that $c_{\mathbf{k}}$ and $U_{\mathbf{k}}$ in principle should carry a ν index, but it is left everywhere implicit, to avoid clutter). The projection operator $\mathcal{P}_{\nu}(\mathbf{k})$ onto the Kramers pair of bands denoted by ν takes the form

$$\mathcal{P}_{\nu}(\mathbf{k}) = \sum_{\sigma} |\mathbf{k},\nu,\sigma\rangle\langle\mathbf{k},\nu,\sigma| = U_{\mathbf{k}}U_{\mathbf{k}}^{\dagger}. \tag{21}$$

Projecting the irreducible pairing matrices $\vec{M}$ and $\vec{N}(\mathbf{k})$ onto the valence band basis yields 2×2 pairing matrices, which we denote $\vec{m}(\mathbf{k})$ and $\vec{n}(\mathbf{k})$, respectively. The latter are obtained from the $\vec{M}$ and $\vec{N}(\mathbf{k})$ matrices by

$$\vec{m}(\mathbf{k}) = U_{\mathbf{k}}^{\dagger}\vec{M}U_{\mathbf{k}}, \quad \vec{n}(\mathbf{k}) = U_{\mathbf{k}}^{\dagger}\vec{N}(\mathbf{k})U_{\mathbf{k}}. \tag{22}$$

Note that generally lower case symbols denote the projected version of the higher case ones (with their ν dependence suppressed).

The projection procedure performed by Eq. (21) can also be expressed in a form which does not require choosing a basis for the doubly degenerate valence band states. Using the Hamiltonian of Eq. (4) it is straightforward to establish that the 4×4 form of the projection operator $\mathcal{P}_{\nu}(\mathbf{k})$ onto the ν bands is given by

$$\mathrm{P}_{\nu}(\mathbf{k}) = \frac{1}{2} + \frac{\nu}{2E_{\mathbf{k}}}\left(c_1\sum_{a=1}^{3} d_a(\mathbf{k})\Gamma_a + c_2\sum_{a=4}^{5} d_a(\mathbf{k})\Gamma_a\right). \tag{23}$$

Note that in the presence of spherical symmetry (i.e., $c_1 = c_2$ and $c_3 = 0$), Eq. (23) simply becomes $\frac{1}{2} + \frac{\nu c_1}{2E_{\mathbf{k}}}\sum_{a=1}^{5} d_a(\mathbf{k})\Gamma_a$, and the band *index* ν can be traded for $3/2$ ($\nu\,\mathrm{sgn}c_1 = 1$) or $1/2$ ($\nu\,\mathrm{sgn}c_1 = -1$), i.e., $\mathrm{P}_{3/2}(\mathbf{k}) = \frac{1}{2} + \frac{|c_1|}{2E_{\mathbf{k}}}\sum_{a=1}^{5} d_a(\mathbf{k})\Gamma_a$ and $\mathrm{P}_{1/2}(\mathbf{k}) = \frac{1}{2} - \frac{|c_1|}{2E_{\mathbf{k}}}\sum_{a=1}^{5} d_a(\mathbf{k})\Gamma_a$.

It is worth highlighting that the projection operators have the full symmetry of the normal state system. Consequently, the representation labels—quantum number J in spherical symmetry—which characterize the irreducible pairing channels remain good quantum numbers after projection. A remark concerning the spin quantum number S is in order, however. Within the valence band, which is twofold pseudospin degenerate, only pseudospin-"singlet" and pseudospin-"triplet" pairings can be formed. As a result, Fermi statistics mandates that the $S = 2$ and $S = 3$ spin pairing channels project onto the pseudospin-singlet ($\propto\sigma^0$) and pseudospin-triplet ($\propto\sigma^{\mu}$) channels, respectively. The multicomponent structure of the $S = 2$ and $S = 3$ spin pairing channels is then reflected in (additional) momentum dependence after projection onto the valence band. To see this in practice, consider the $(L,S) = (0,2)$ pairing channel. The five pairing matrices $\vec{M}_{J=S=2}$ simply project onto the five d-wave spherical harmonics $Y_{l=2}^{m}(\hat{\mathbf{k}})$, where l is the orbital angular momentum. Specifically, the projected pairing matrices $\vec{m}_{S=2}(\mathbf{k})$ are given by

$$m_{S=2}^{m}(\hat{\mathbf{k}}) = \pm Y_{l=2}^{m}(\hat{\mathbf{k}})I_2. \tag{24}$$

In cubic symmetry, where $J = S = 2$ splits into E_g and T_{2g}, these projected pairings become

$$m_{1,2,3}(\hat{\mathbf{k}}) = \pm c_1 \frac{d_{1,2,3}(\mathbf{k})}{E_{\mathbf{k}}} I_2, \quad m_{4,5}(\hat{\mathbf{k}}) = \pm c_2 \frac{d_{4,5}(\mathbf{k})}{E_{\mathbf{k}}} I_2. \tag{25}$$

We observe that, as a consequence of projecting onto the Fermi surface bands, only the parity of S is a good quantum number. As a result, channels with equal J but different (L,S) can mix after projection. More specifically, if $\vec{n}_J(\mathbf{k})$ and $\vec{n}'_J(\mathbf{k})$ are two sets of projected pairing matrices, obtained from channels with different (L,S), they are not necessarily orthogonal. This mixing of channels with different spin and orbital quantum numbers can occur since projection onto the Fermi surface implies ignoring all pair scattering terms which involve the conduction band states. All interband and intraconduction band pair scattering terms are projected out, and therefore, the information retained is not sufficient to distinguish the quantum numbers L and S.

This happens in particular when projecting the channel with nontrivial orbital angular momentum $L = 1$ and spin angular momentum $S = 1$ and $S = 3$. Both can form a total angular momentum $J = 2$. In such cases we will explicitly add a label to the different *unprojected* representations, which project into the same representation J by an additional index j, for example $N_{J=2,j}(\mathbf{k})$ labels the two $S = 1$ and $S = 3$, which project to the same representation.

Now, inserting $\mathrm{Id} = \sum_\nu \mathcal{P}_\nu$ in Eqs. (3) and (16), keeping only the terms within a set of bands, and using the spherical symmetry formulation, we obtain the effective action for the two bands which intercept the Fermi energy:

$$\begin{aligned}\mathcal{S}^{\mathrm{eff}} = &\sum_k c_k^\dagger (\mathsf{E}_\nu(\mathbf{k}) - i\omega) c_k \\ &+ \frac{1}{8}\frac{1}{\beta \mathcal{V}} \sum_{\mathbf{k},\mathbf{k}',\omega,\omega'} \sum_J \hat{V}^J_{\alpha\beta\gamma\delta}(\mathbf{k},\mathbf{k}';\omega-\omega') \\ &\times c^\dagger_{k\alpha} c^\dagger_{-k\beta} c_{-k'\gamma} c_{k'\delta},\end{aligned} \tag{26}$$

where

$$\begin{aligned}&\hat{V}^J_{\alpha\beta\gamma\delta}(\mathbf{k},\mathbf{k}';\omega-\omega') \\ &\quad = V_J(\omega-\omega')[\vec{n}_J(\mathbf{k})(i\sigma^y)]_{\alpha\beta} \cdot [(-i\sigma^y)\vec{n}^\dagger_J(\mathbf{k}')]_{\gamma\delta},\end{aligned} \tag{27}$$

where $V_J = V_{0,1}$ [from Eq. (15)] for J coming from S even or S odd, respectively. Like in Eq. (17), the sum over J runs over even and odd pairing channels, and $\vec{n}_J(\mathbf{k}) = \vec{m}_S$ for S even. Equation (27) is essentially Eq. (17) with the replacements $M \to m$, $N \to n$, $\gamma \to (i\sigma^y)$, $\psi \to c$.

As mentioned above, the sum over even S matrices involves only the 2×2 identity matrix and can be written explicitly:

$$\frac{1}{2}\left(1 + \frac{c_1^2 \sum_a d_a(\mathbf{k}) d_a(\mathbf{k}')}{E_{\mathbf{k}} E_{\mathbf{k}'}}\right)[c_k^\dagger i\sigma^y (c^\dagger_{-k})^T][(i\sigma^y c_{-k'})^T c_{k'}]. \tag{28}$$

This (basis-dependent since the bands are degenerate) expression is useful to gain insight into the effect of the projection operators, but in practice the actual diagonalization is not necessary, since only the trace of the projected matrices appears in our calculations, and we have the relation

$$\mathrm{Tr}\big[n^\alpha_J(\hat{\mathbf{k}}) n^{\alpha'\dagger}_{J'}(\hat{\mathbf{k}})\big] = \mathrm{Tr}\big[\mathrm{P}_\nu(\mathbf{k}) N^\alpha_J(\hat{\mathbf{k}}) \mathrm{P}_\nu(\mathbf{k}) N^{\alpha'\dagger}_{J'}(\hat{\mathbf{k}})\big]. \tag{29}$$

Therefore we will only be formally assuming a diagonalization of the Hamiltonian, but directly computing the right-hand side of Eq. (29) using the general explicit expression Eq. (23), which allows us to perform all analytical calculations.

V. LINEARIZED ELIASHBERG THEORY

We are now in a position to analyze the superconducting instabilities based on a general formalism for the derivation of the transition temperature in spin-orbit coupled multiband systems with nontrivial structure. Our approach relies on Eliashberg theory, the equations of which we derive from the lowest-order self-energy correction due to the interaction, in the presence of superconducting test vertices. Such a scheme corresponds to neglecting vertex corrections at all orders and is equivalent to Dyson's equation truncated at first order in the interaction.

Here we will present the main steps of our analysis, relegating most of the details to the Appendices. Furthermore, in our *presentation*, we will consider spherical symmetry, and, for concreteness, focus specifically on a hole Fermi surface (with pseudospin $\pm\frac{3}{2}$ states), which is relevant for existing experiments on YPtBi.

To obtain the Eliashberg equations starting from the projected effective action of Eq. (26), we introduce a superconducting test vertex Σ_A. Specifically, we rearrange the normal part and interaction part of the action $\mathcal{S}_0$ and $\mathcal{S}_{\mathrm{int}}$ as [39]

$$\begin{aligned}\mathcal{S}_0 &\to \mathcal{S}'_0 = \mathcal{S}_0 - \mathcal{S}_A, \\ \mathcal{S}_{\mathrm{int}} &\to \mathcal{S}'_{\mathrm{int}} = \mathcal{S}_{\mathrm{int}} + \mathcal{S}_A,\end{aligned}$$

where the anomalous part $\mathcal{S}_A$ contains the test vertex $\Sigma_A = \Sigma_A(\mathbf{k},\omega)$ and takes the form

$$\mathcal{S}_A = \frac{1}{2}\sum_k \sum_{a,b} c^\dagger_{ka}(\Sigma_A i\sigma^y)_{ab} c^\dagger_{-kb} + \mathrm{H.c.} \tag{30}$$

Here a,b label the pseudospin degree of freedom $\pm\frac{3}{2}$. [Recall that $k = (\mathbf{k},\omega)$.] A self-consistent equation for the pairing test vertex Σ_A is then obtained by setting $\langle \mathcal{S}'_{\mathrm{int}} \rangle_{\mathcal{S}'_0} = 0$, where $\langle X \rangle_{\mathcal{S}'_0} \equiv \int Dc Dc^\dagger X e^{-\mathcal{S}'_0}$. Diagrammatically, the self-consistent equation $\langle \mathcal{S}'_{\mathrm{int}} \rangle_{\mathcal{S}'_0} = 0$ can be represented as in Fig. 2. Solving the self-consistent equation is then equivalent to solving a linearized gap equation for T_c.

FIG. 2. Diagrammatic representation of the Eliashberg equation. The solid lines are fermion propagators $\langle C_{k,a} C^\dagger_{k,b} \rangle_{\mathcal{S}'_0}$, where C_k is the Nambu spinor of Eq. (31). The dashed line represents the interaction V.

For practical purposes it is convenient to adopt the Nambu spinor formalism and define

$$C_k = \begin{pmatrix} c_k \\ i\sigma^y (c^\dagger_{-k})^T \end{pmatrix}. \tag{31}$$

The normal part of the action $\mathcal{S}_0$ can then be expressed as

$$\mathcal{S}_0 = \frac{1}{2}\sum_k C^\dagger_k \begin{pmatrix} \mathsf{E}_- - i\omega & \\ & -\mathsf{E}_- - i\omega \end{pmatrix} C_k, \tag{32}$$

where $\mathsf{E}_- = \mathsf{E}_-(\mathbf{k})$ is the negative energy branch of the spectrum. The interaction part of the action takes the form

$$\mathcal{S}_{\rm int} = \frac{1}{32}\frac{1}{\beta\mathcal{V}}\sum_{k,k'}\sum_J V_J(\omega-\omega') \times [C^\dagger_k \vec{n}_J(\mathbf{k})\tau^+ C_k]\cdot[C^\dagger_{k'}\vec{n}^\dagger_J(\mathbf{k}')\tau^- C_{k'}], \tag{33}$$

where $\tau^\pm = \tau^x \pm i\tau^y$, and the Pauli matrices $\tau^{x,y,z}$ act on the Nambu spinor index. Finally, the anomalous part $\mathcal{S}_A$ takes the simple off-diagonal form

$$\mathcal{S}_A = \frac{1}{2}\sum_k C^\dagger_k \begin{pmatrix} & \Sigma_A \\ \Sigma^\dagger_A & \end{pmatrix} C_k. \tag{34}$$

We can now calculate $\langle \mathcal{S}'_{\rm int}\rangle_{\mathcal{S}'_0}$ using Wick's theorem, expressing the quartic interaction in products of Nambu propagators $G^{ab} = \langle C_{k,a} C^\dagger_{k,b}\rangle_{\mathcal{S}'_0}$. The Green's function G has a matrix structure both in Nambu and pseudospin space, i.e.,

$$\begin{pmatrix} G_{11} & G_{12} \\ G_{21} & G_{22} \end{pmatrix} = \mathcal{K}\begin{pmatrix} \langle c_k c^\dagger_k\rangle & \langle c_k (c_{-k})^T\rangle \\ \langle (c^\dagger_{-k})^T c^\dagger_k\rangle & -\langle c_{-k} c^\dagger_{-k}\rangle^T \end{pmatrix}\mathcal{K}^\dagger, \tag{35}$$

where $\mathcal{K} = \mathrm{Diag}(1, i\sigma^y)$ and $\langle\cdots\rangle = \langle\cdots\rangle_{\mathcal{S}'_0}$. [Note that in Eq. (35) the matrix elements on the right-hand side should themselves be understood to be matrices: $\langle c_k c^\dagger_k\rangle$ is for example to be read as $\langle c_{k,a} c^\dagger_{k,b}\rangle$, and not as $\sum_a \langle c_{k,a} c^\dagger_{k,a}\rangle$.] Since $\mathcal{S}'_0$ is quadratic in the Nambu operators, the Green's function G can be straightforwardly found to be

$$G(\mathbf{k},\omega) = \frac{i\omega\tau^0 + \mathsf{E}_-\tau^z - \Sigma_A\tau^x}{\omega^2 + \mathsf{E}_-^2 + \mathrm{Tr}\Sigma_A^2}, \tag{36}$$

with the off-diagonal part given by

$$G_{21}(\mathbf{k},\omega) = -\frac{\Sigma_A}{\omega^2 + \mathsf{E}_-^2 + \mathrm{Tr}\Sigma_A^2}. \tag{37}$$

Then, the linearized Eliashberg equation shown diagrammatically in Fig. 2 takes the form

$$\Sigma_A(\mathbf{k},\omega) = \frac{1}{4\beta\mathcal{V}}\sum_{\mathbf{k}',\omega'}\sum_J V_J(\omega-\omega') \times \mathrm{Tr}[G_{12}(\mathbf{k}',\omega')(-i\sigma^y) n^\dagger_J(\mathbf{k}')] n_J(\mathbf{k}). \tag{38}$$

Here we assumed a purely real pairing and assumed proximity to the transition temperature where $\mathrm{Tr}\Sigma_A^2$ is small and can be neglected.

A. Solving for T_c: Spherical symmetry

Let us consider first the case of full spherical symmetry. We linearize the dispersion near the Fermi energy and perform the integration over momentum analytically. As explained in Sec. IV there are in general two cases to consider. Let us first consider the simpler case, where the total angular momentum representation J derives from a unique set of quantum numbers L and S. In that case, we may consider a pairing function of the form $\Sigma_A(\mathbf{k},\omega) = \Delta(\omega) n^\alpha_J(\mathbf{k})$ where $\Delta(\omega)$ is a scalar and $\alpha = 1,\ldots,2J+1$. The Eliashberg equation then assumes the form

$$\Delta_J(\omega) = -\frac{\pi}{\beta_{c,J}}\sum_{\omega'} K_J(\omega,\omega')\Delta_J(\omega'), \tag{39}$$

where

$$K_J(\omega,\omega') = \int \frac{d\mathbf{k}'}{(2\pi)^3}\frac{1}{4} V_J(\omega-\omega') \times \frac{\mathrm{Tr}\left[\mathrm{P}_-(\mathbf{k}') N^\alpha_J(\mathbf{k}')\mathrm{P}_-(\mathbf{k}') N^{\alpha\,\dagger}_J(\mathbf{k}')\right]}{\omega'^2 + \mathsf{E}_-^2(\mathbf{k}')} = \frac{A_J}{2|\omega'|} f_{0,1}[\eta(\omega-\omega')], \tag{40}$$

where the interaction V was taken as in Eq. (6) with the electronic polarization function in the Thomas-Fermi approximation, and the dispersion was linearized close to the Fermi surface.

The strength of the attraction, encoded in the kernel K_J, is dictated by two factors. The first is the representation dependent constant:

$$A_J = \frac{1}{4}\int \frac{d\hat{\mathbf{k}}}{4\pi}\mathrm{Tr}\left[\mathrm{P}_\nu(\mathbf{k}) N^\alpha_J(\hat{\mathbf{k}})\mathrm{P}_\nu(\mathbf{k}) N^{\alpha\,\dagger}_J(\hat{\mathbf{k}})\right], \tag{41}$$

which can be found in Table III for both 3/2 and 1/2 bands (note that this constant is the same for all $\alpha = 1,\ldots,2J+1$

TABLE III. Strength of the projected pairing channels up to one power of k in spherical symmetry [$O(3)$], $A_J = \frac{1}{4}\int\frac{d\hat{\mathbf{k}}}{4\pi}\mathrm{Tr}[\mathrm{P}_\nu(\mathbf{k})N^\alpha_J(\hat{\mathbf{k}})\mathrm{P}_\nu(\mathbf{k})N^{\alpha\,\dagger}_J(\hat{\mathbf{k}})]$. (L,S,J) stand for momentum (the power of $\mathbf{k}$), spin, and their sum (i.e., total-angular momentum), respectively. Since we consider only local and single power of $\mathbf{k}$ pairing, only $L=0$ and $L=1$ appear (in principle L can take all integer values). The parity (even/odd) of each channel is given by $(-1)^L$. The bolded numbers mark the channels with highest non-s-wave pairing. Note that, after projection, the channels (1,1,2) and (1,3,2) mix. The corresponding matrix elements $A^{ii'}_J = \frac{1}{4}\int\frac{d\hat{\mathbf{k}}}{4\pi}\mathrm{Tr}[\mathrm{P}_\nu(\mathbf{k})N^\alpha_{J,i}(\hat{\mathbf{k}})\mathrm{P}_\nu(\mathbf{k})N^{\alpha\,\dagger}_{J,i'}(\hat{\mathbf{k}})]$ are given on the fifth row of the table. The corresponding coupling strength is obtained by the largest eigenvalue of the matrix (see text).

L	S	J	$\lvert\mathbf{k},3/2,\sigma\rangle$	$\lvert\mathbf{k},1/2,\sigma\rangle$
0	0	0	1/2	1/2
0	2	2	1/10	1/10
1	1	0	**9/10**	1/10
1	1	1	0	2/5
1	1,3	2	$\frac{9}{25}\begin{pmatrix} 1 & \frac{-1}{\sqrt{14}} \\ \frac{-1}{\sqrt{14}} & 1/14 \end{pmatrix}$	$\frac{1}{25}\begin{pmatrix} \mathbf{7} & \frac{33}{\sqrt{14}} \\ \frac{33}{\sqrt{14}} & \mathbf{177/14} \end{pmatrix}$
1	3	3	**9/14**	3/70
1	3	4	13/70	27/70

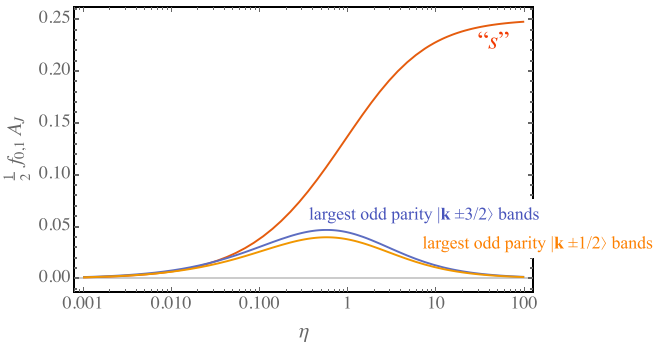

FIG. 3. The value $\frac{1}{2} f_{0,1} A$ which controls the coupling strength of the Eliashberg equations as a function of the parameter η defined in Eq. (44) for the screened Coulomb interaction $V(\mathbf{q},\omega) = 4\pi e^2/\{[\varepsilon_\infty + \varepsilon_c(\omega)]q^2 + 8\pi e^2 N(0)\}$. We assume spherical symmetry and particle-hole symmetric bands. For the usual *non*-spin-orbit coupled parabolic bands, the large-η limit of $\frac{1}{2} f_0 A_0$ is 0.5, as compared to 0.25 in the present case.

at any given J). The second are the functions

$$f_0(\eta) = \frac{\eta}{2} \ln\left(1 + \frac{2}{\eta}\right), \tag{42}$$

$$f_1(\eta) = \frac{\eta}{2}\left[-2 + (1+\eta)\ln\left(1 + \frac{2}{\eta}\right)\right]. \tag{43}$$

Here 0 or 1 correspond to the even and odd representations of J, respectively, and the parameter η quantifies the strength of the Coulomb interaction and is given by

$$\eta(\omega) = \frac{q_{\mathrm{TF}}^2(\omega)}{2k_{\mathrm{F}}^2}, \tag{44}$$

where $q_{\mathrm{TF}}(\omega) = \sqrt{8\pi e^2 N(0)/[\varepsilon_\infty + \varepsilon_c(\omega)]}$ is the frequency-dependent Thomas-Fermi momentum. These two factors, A_J and $f_{0,1}(\eta)$, multiplied together are plotted as a function of η in Fig. 3 for the three examples which give the highest coupling strength: $J = 0$ even (s wave) in red, $J = 0$ odd in the hole band (p wave) in blue, $J = 2$ odd in the electron band (p wave) in orange.

From Eq. (40) we find that the functions $f_{0,1}(\eta)$ depend on frequency only via the parameter η. At high frequencies the functions saturate to the value $f_{0,1}(\eta_\infty)$ and continuously go to $f_{0,1}(\eta_0)$ at zero frequency, where $\eta_\infty = \lim_{\omega\to\infty} q_{\mathrm{TF}}^2(\omega)/(2k_{\mathrm{F}}^2)$ and $\eta_0 = q_{\mathrm{TF}}^2(0)/(2k_{\mathrm{F}}^2)$.

This allows us to understand how attraction appears, leading to superconductivity, and to put bounds on the transition temperature T_c as follows. As is usual, the interaction $V(\omega)$ can be decomposed into a static repulsion μ (the high-frequency limit of the interaction) and an attractive part λ such that

$$V_J(\omega) = \mu_J - \lambda_J(\omega) \tag{45}$$

and

$$\mu_J = \lim_{\omega\to+\infty} V_J(\omega), \tag{46}$$

which also defines $\lambda_J(\omega)$. Upon considering a low-energy theory, and therefore integrating out large frequencies, the static repulsion μ_J is renormalized to a small dimensionless repulsion μ_J^* so long as the Fermi energy is large compared to the phonon frequency, which is the case for YPtBi. On the other hand, $\lambda_J(\omega)$, which represents only the attraction due to the electron-phonon interaction, can be considered to be largely unaffected by large-frequency effects. From here on we set μ_J^* to be zero (as in standard BCS theory), so that now $V_J(\omega) \to -\lambda_J(\omega)$. We can then read off the low frequency attractive part of the interaction

$$\lambda_J = \lambda_J(\omega = 0) = \frac{A_J}{2}[f_{0,1}(\eta_\infty) - f_{0,1}(\eta_0)]. \tag{47}$$

Given $\varepsilon_c(\infty) < \varepsilon_c(0)$, we have $\eta_\infty > \eta_0$, so that $\lambda_J > 0$ in the s-wave channel as well as in the odd parity channels if η_∞ is not too large. The transition temperature in channel J is then bound from above by $T_{c,J} < \omega_L \exp[-1/\lambda_J]$.

Finally, we note that in the case of 1/2-band doping (electron doping in the YPtBi case) the highest coupling constant is obtained in the case where two sets of quantum numbers L and S mix, namely the case of of $L = 1$, $S = 1$, and $S = 3$, which both project into the odd $J = 2$ representation. Let us now describe how to deal with this more complicated situation. As explained in Sec. IV the group elements $N_2^\alpha(\mathbf{k})$ are now labeled by an additional index i, which accounts for the $S = 1$ or $S = 3$ origin. The constant Eq. (41) is then generalized to

$$A_J^{ii'} = \frac{1}{4}\int \frac{d\hat{\mathbf{k}}}{4\pi} \mathrm{Tr}\left[\mathrm{P}_\nu(\mathbf{k}) N_{J,i}^\alpha(\hat{\mathbf{k}}) \mathrm{P}_\nu(\mathbf{k}) N_{J,i'}^{\alpha\,\dagger}(\hat{\mathbf{k}})\right] \tag{48}$$

and forms a 2×2 matrix (see the fifth row in Table III). $\Delta(\omega) n_{J,i}^\alpha(\mathbf{k})$ alone cannot solve the self-consistent equation (38), but now a mixture of the two $n_{2,i}^\alpha(\mathbf{k})$ can be used. Defining

$$\Sigma_A(k) = \Delta(\omega) \sum_{i=1,2} \phi_i n_{2,i}^\alpha(\mathbf{k}) \tag{49}$$

(i.e., not introducing additional $\mathbf{k}$ dependence in the coefficients ϕ_i), we find that a set of solutions is given by solving for the eigenvalues and eigenvectors of the matrix $\mathbf{A}_J = (A_j^{ii'})_{ii'}$ (the fifth row of Table III)—see Appendix D. For the 1/2 bands, the largest coupling constant, i.e., that which will yield the largest T_c, is $\frac{1}{140}(55 + \sqrt{2689}) \approx 0.76$, and is obtained for a pairing matrix equal to $0.59 n_{J=2,S=1}^\alpha + 0.81 n_{J=2,S=3}^\alpha$. The other eigenvalues are given in Table III, and corresponding eigenvectors in the Appendix D.

B. General discussion of the results

By estimating the coupling strengths in each symmetry channel we find the following results:

(i) Looking at the first row of Table III, we find that in the case of s-wave pairing the constant dictating the coupling strength in the s-wave channel A_0 is equal to 1/2. This should be compared with the analysis of GLF [32], where a simple quadratic band without spin-orbit coupling was studied. In their case, calculating the same constant gives $A_0 = 1$ (note that this would be true even if the number of bands were to be multiplied by 2 to match the current case). Thus, we find that the effectiveness of a local attraction in generating s-wave pairing is dramatically reduced. One way to see this is by considering the finely tuned point $\alpha_2 = \alpha_3 = \alpha_4 = 0$ in Eq. (3). There, all four bands are degenerate, the Fermi energy

therefore crosses all four bands, so that no projection onto a subset of the latter should be performed, and $A_0 = 1$.

(ii) We find an explicit difference between the electron and hole bands in the odd-parity pairing coupling strengths as shown in Table III. The extreme example is the pairing in the $J = 1$ representation, which is only allowed in the 1/2 bands [40]. Therefore the largest odd-parity pairings occur in different channels for hole and electron bands, an observation which could in principle be verified experimentally in systems which display odd-parity superconductivity, by changing the carrier type. Of course, various characteristics of the bands, and notably the density of states, which may greatly vary between the electron and whole bands, will however play a major role in determining the *quantitative* values of the pairings, but should not modify the hierarchy of the channels for a given carrier type.

(iii) The highest T_c for nontrivial pairing in the 3/2 bands (which is physically relevant for YPtBi) is obtained for the $L = 1$, $S = 1$, $J = 0$ [corresponding to $N_0(\mathbf{k}) \propto \mathbf{k} \cdot \mathbf{J}$] and the $L = 1$, $S = 3$, and $J = 3$ [corresponding to Eq. (B6)] channels, where the former is a one-dimensional representation and the latter is a five-dimensional one, allowing for the possibility of time-reversal symmetry breaking. This means, in particular, that the largest non-s-wave pairing occurs in a *nonlocal* channel, in contrast with what has been considered in several works.

The *local* pairing states (with $L = 0$ and $S = 0,2$, i.e., rows 1, 2, and 3 in Table I) were studied in detail in Refs. [41–43]. We leave the analysis of the odd-parity pairing states from Table II, in particular the ones we find are favored by the polar-phonon mechanism, to future study.

C. Application to YPtBi, and factors that may favor non-s-wave pairing

In the previous section we found that the density-density interaction Eq. (6) favored s-wave pairing. However, s-wave pairing is not consistent with recent penetration depth measurements [26], which seem to indicate the existence of nodes [29,44]. In this short section we first review the effect of Fermi liquid corrections, which may enhance T_c, and effects beyond RPA, which may favor odd-parity pairing.

The coupling strength can be enhanced when strong Fermi-liquid theory corrections are present. In particular the compressibility of a charged Fermi liquid is reduced by the Landau parameter F_0^s. As a result q_{TF} is also reduced and the interaction Eq. (6) is modified in the low frequency limit

$$V(\omega, \mathbf{q}) = \frac{1 + F_0^s}{2N(0)} \frac{\tilde{q}_{\mathrm{TF}}^2(\omega)}{q^2 + \tilde{q}_{\mathrm{TF}}^2(\omega)}, \tag{50}$$

where $\tilde{q}_{\mathrm{TF}}^2(\omega) = q_{\mathrm{TF}}^2(\omega)/(1 + F_0^s)$. Thus, the coupling strength is enhanced by a factor of $1 + F_0^s$. Taking $\omega_L \approx 400$ K, we find that to explain the measured $T_c = 0.77$ K in YPtBi one needs $F_0^s = 2.2$, which is a large, but not unrealistic, correction.

We now discuss the how p-wave pairings may overcome s wave. First, we note that RPA relies on linear response. Namely, the response of the electronic polarization, taken into account in Eq. (7), is taken to be linear. This breaks down at short distances much smaller than the screening core (of radius $r_{\mathrm{TF}} = 2\pi/q_{\mathrm{TF}}$), where the electric field becomes large. To correct for this, we consider an additional *local* interaction

$$\delta \mathcal{S}_{\mathrm{int}} = \frac{\delta V}{2} \int_x \psi_x^\dagger \psi_x \psi_x^\dagger \psi_x. \tag{51}$$

When $\delta V > 0$ it enhances the repulsion, but only in the even parity pairing channels (i.e., $L = 0$). Thus, in this case it favors p-wave pairing due to enhanced local repulsion, i.e., by penalizing s-wave pairing. However, even if the strength of the s-wave pairing is reduced, this is not enough to account for the T_c observed in experiment [19], because the coupling in the $L = 1$, $S = 0$, and $J = 0$ channel is too weak. Indeed, in the $L = 1, S = 1, J = 0$ channel, the maximal value the coupling constant can take is $\lambda \approx 0.05$. This is not enough to explain the transition temperature in YPtBi, for example. It is however a non-negligible contribution. Strong cubic asymmetry, and a stronger momentum dependence of the interaction, is likely to enhance the nonlocal channels considerably, as we point out below.

D. Cubic symmetry

Like before, our derivation carries over to cubic symmetry. In particular Eq. (38) and the first equality of Eq. (40) are still valid with the replacement of the index J by the cubic representations listed in Tables I and II. However, no simple form such as the second equality of Eq. (40) exists in that case. Indeed, there, we made use of the isotropy of E_-—which is no longer true in cubic symmetry. All of the angular dependence was then carried only by the factor $\mathrm{Tr}[\mathrm{P}_-(\mathbf{k}')N_J^\alpha(\hat{\mathbf{k}}')\mathrm{P}_-(\mathbf{k}')N_J^{\alpha\dagger}(\hat{\mathbf{k}}')]$, which itself did not depend on the magnitude of $\mathbf{k}'$, but only its direction. In cubic symmetry, no such trivial separation of the dependencies on the direction and magnitude of $\mathbf{k}$ exists. In that case, the coefficients A_R will carry no real meaning, and one needs to resort to numerical estimates of the full $d\mathbf{k}'$ integral for each set of parameter values. Physically, because of the additional angular dependence in the integral, one expects this will typically tend to enhance the odd parity pairings, but it seems not enough to overcome that of the s wave. However, together with a stronger momentum dependence of the dielectric constant, such as that describing plasmons, one can reasonably expect that nonlocal pairings become large enough to induce superconductivity and dominant.

It is also worth noting that, in cubic symmetry, mixing of several representation copies is the rule rather than the exception (as was the case in spherical symmetry where only $J = 2$, $L = 1$, and $S = 1,3$ mixed), because most representations appear several times.

VI. DISCUSSION

We have presented a theory for the study of superconductivity in spin-orbit coupled materials and applied it to $j = \frac{3}{2}$ semimetals in three dimensions. In doing so, we classified all possible pairing channels, which are local or linear in momentum.

Our study led us to a few general results. First we found that the coupling strengths were nontrivial in each channel: even in the s-wave one the quadratic band touching case differs from

that of non-spin-orbit coupled bands. We also showed that the pairing strength and the resulting expected gap symmetry was different in the case of electron and hole doping. Thus, we expect that the superconducting state in an electron-doped half-Heusler will be different than in the hole doped ones.

We used our theory to study the pairing strengths in each channel due to a polar optical phonon as first discussed by GLF [32]. We showed that the coupling strength can potentially be large enough to explain superconductivity in the half-Heuslers, in contrast to the conclusion of Ref. [28].

Within RPA we found that the highest T_c was in the s-wave channel, but that several odd-parity channels had non-negligible pairings. As we pointed out, corrections which go beyond linear response may favor pairing in these channels. It is important to note however, that the full dynamical and momentum dependence of the dielectric constant Eq. (7) needs to be taken into account to be able to make better estimates of the coupling constants. We expect that a strong momentum dependence of the interaction, such as that introduced by plasmons, is likely to substantially enhance T_c in nonlocal channels. We leave this to future study.

ACKNOWLEDGMENTS

We thank Leon Balents, Max Metlitski, and Doug Scalapino for useful discussions. L.S. also acknowledges Leon Balents and Eun-Gook Moon for a prior collaboration on a related topic. L.S. and J.R. were supported by the Gordon and Betty Moore Foundation through scholarships of the EPiQS initiative under Grant No. GBMF4303. L.S. also acknowledges the hospitality of the KITP, where part of this work was carried out, and NSF Grant PHY-1125915. P.A.L. was supported by the DOE under Grant No. FG02-03ER46076. L.F. and J.W.F.V. acknowledge funding by the DOE Office of Basic Energy Sciences, Division of Materials Sciences and Engineering under Award No. DE-SC0010526.

APPENDIX A: DEFINITIONS AND PARAMETER VALUES

The Fourier and Matsubara transformations (ω is a fermionic Matsubara frequency, $\omega = \omega_n = \frac{(2n+1)\pi}{\beta}$) are carried out using the following normalization:

$$\psi_x = \frac{1}{\sqrt{\beta}\sqrt{\mathcal{V}}} \sum_{\omega,\mathbf{k}} e^{i\mathbf{k}\cdot\mathbf{r}-i\omega\tau}\psi_k. \tag{A1}$$

1. Hamiltonian definitions

The fermionic Hamiltonian density reads

$$\mathcal{H}_0(\mathbf{k}) = \alpha_1\mathbf{k}^2 + \alpha_2(\mathbf{k}\cdot\mathbf{J})^2 + \alpha_3\left(k_x^2J_x^2 + k_y^2J_y^2 + k_z^2J_z^2\right) + \alpha_4\mathbf{k}\cdot\mathbf{T} - \mu \tag{A2}$$

$$= c_0\mathbf{k}^2 + \sum_{a=1}^{5}\hat{c}_a d_a(\mathbf{k})\Gamma_a + c_3\mathbf{k}\cdot\mathbf{T} - \mu, \tag{A3}$$

where $\hat{c}_1 = \hat{c}_2 = \hat{c}_3 = c_1$ and $\hat{c}_4 = \hat{c}_5 = c_2$. The first line uses the conventional Luttinger parameters ($\alpha_{1,2,3}$) in the $j = \frac{3}{2}$ matrix representation [6], and the second line is the form used in the main text. The Gamma matrices (Γ_a) form a Clifford algebra, $\{\Gamma_a,\Gamma_b\} = 2\delta_{ab}$, and have been introduced as described in the literature [45], and

$$d_1(\mathbf{k}) = \frac{k_xk_y}{\sqrt{2}}, \quad d_2(\mathbf{k}) = \frac{k_xk_z}{\sqrt{2}}, \quad d_3(\mathbf{k}) = \frac{k_yk_z}{\sqrt{2}},$$
$$d_4(\mathbf{k}) = \frac{k_x^2-k_y^2}{2\sqrt{2}}, \quad d_5(\mathbf{k}) = \frac{2k_z^2-k_x^2-k_y^2}{2\sqrt{6}}.$$

Note that c_0 (α_1) quantifies the particle-hole asymmetry, while $|c_1 - c_2|$ (α_3) naturally characterizes the cubic anisotropy and c_3 (α_4) the departure from inversion symmetry. In the absence of inversion breaking, i.e., when $c_3 = 0$, the energy eigenvalues are $\mathsf{E}_\pm(\mathbf{k}) = c_0\mathbf{k}^2 \pm E(\mathbf{k}) - \mu$, where $E(\mathbf{k}) = \sqrt{\sum_{a=1}^{5}\hat{c}_a^2 d_a^2(\mathbf{k})}$ and the Hamiltonian density can be rewritten

$$\mathcal{H}_0^{\text{inv}}(\mathbf{k}) = \sum_{\nu=\pm1}\mathsf{E}_\nu(\mathbf{k})\mathrm{P}_\nu(\mathbf{k}), \tag{A4}$$

where $\mathrm{P}_\nu(\mathbf{k}) = \frac{1}{2}(1 + \nu\frac{\mathcal{H}_0(\mathbf{k})-c_0\mathbf{k}^2+\mu}{E(\mathbf{k})})$ is a projection operator, $\mathrm{P}_\nu^2(\mathbf{k}) = \mathrm{P}_\nu(\mathbf{k})$ (no summation).

It is straightforward to relate the c_i coefficients used in Eq. (A3) to the Luttinger α_i parameters used in Eq. (A2). This can be done by expressing the spin operators in terms of the Gamma matrices, using for example the equalities

$$J_x = \frac{\sqrt{3}}{2}\Gamma_{15} - \frac{1}{2}(\Gamma_{23} - \Gamma_{14}),$$
$$J_y = -\frac{\sqrt{3}}{2}\Gamma_{25} + \frac{1}{2}(\Gamma_{13} + \Gamma_{24}), \quad J_z = -\Gamma_{34} - \frac{1}{2}\Gamma_{12}, \tag{A5}$$

where $\Gamma_{ab} = \frac{1}{2i}[\Gamma_a,\Gamma_b]$. We find

$$\begin{cases} c_0 = \alpha_1 + \frac{5}{4}(\alpha_2+\alpha_3) \\ c_1 = \sqrt{6}\alpha_2 \\ c_2 = \sqrt{6}(\alpha_2+\alpha_3) \\ c_3 = \alpha_4 \end{cases}, \quad \text{i.e.,} \quad \begin{cases} \alpha_1 = c_0 - \frac{5}{4\sqrt{6}}c_2 \\ \alpha_2 = \frac{c_1}{\sqrt{6}} \\ \alpha_3 = \frac{c_2-c_1}{\sqrt{6}} \\ \alpha_4 = c_3 \end{cases}. \tag{A6}$$

Note that if explicit matrices are used, they follow the definitions in Ref. [45]. For these definitions, the 4×4 antisymmetric matrix γ used throughout is equal to $\gamma = -i\Gamma_{13}$.

Finally, the transformation of the d_a under a threefold rotation around the [111] axis is

$$d_1 \to d_2 \to d_3 \to d_1,$$
$$d_4 \to \tfrac{-1}{2}(d_4 + \sqrt{3}d_5), \quad d_5 \to \tfrac{1}{2}(\sqrt{3}d_4 - d_5). \tag{A7}$$

Γ_a transforms like d_a.

a. Spherical symmetry

In spherical symmetry, $c_1 = c_2 = c$ and $c_3 = 0$, and $\alpha_3 = \alpha_4 = 0$. Also the $|j^z = \pm1/2\rangle$ and $|j^z = \pm3/2\rangle$ are good eigenstates, with eigenenergies

$$\mathsf{E}_{1/2}(\mathbf{k}) = \mathbf{k}^2\left(\alpha_1 + \frac{1}{4}\alpha_2\right) = \mathbf{k}^2\left(c_0 - \frac{c}{\sqrt{6}}\right), \tag{A8}$$

$$\mathsf{E}_{3/2}(\mathbf{k}) = \mathbf{k}^2\left(\alpha_1 + \frac{9}{4}\alpha_2\right) = \mathbf{k}^2\left(c_0 + \frac{c}{\sqrt{6}}\right). \tag{A9}$$

In terms of hole and electron bands,

$$\mathsf{E}_{\pm}(\mathbf{k}) = \left(c_0 \pm \frac{|c|}{\sqrt{6}}\right)\mathbf{k}^2. \tag{A10}$$

From these equations, we find the relations between 3/2 and 1/2 bands and $\nu = \pm 1$ electron and hole bands, in spherical symmetry:

$$\begin{aligned} \nu\,\mathrm{sgn}c = -1 &\;\Leftrightarrow\; 1/2 \\ \nu\,\mathrm{sgn}c = +1 &\;\Leftrightarrow\; 3/2 \end{aligned}. \tag{A11}$$

2. Parameter definitions

In Gaussian units ($\pm$ refers to eletron/hole bands), m the effective mass, k_F the Fermi energy, n the carrier density, $N(0)$ the density of states at the Fermi energy, a_0 the effective Bohr radius, q_TF the Thomas-Fermi momentum, Ry the effective Rydberg, and $E_\mathrm{F} = |\mu|$ the Fermi energy are

$$\begin{aligned} m &= \frac{\hbar^2}{2(c_0 \pm |c|/\sqrt{6})} \\ k_\mathrm{F} &= \frac{\sqrt{2mE_F}}{\hbar} = \sqrt{\frac{E_F}{c_0 \pm |c|/\sqrt{6}}} \\ n &= \frac{1}{(2\pi)^3}\frac{4\pi}{3}k_\mathrm{F}^3 = \frac{1}{6\pi^2}\sqrt{\frac{E_F}{c_0 \pm |c|/\sqrt{6}}}^3 \\ N(0) &= \frac{mk_F}{2\pi^2\hbar^2} = \frac{k_F}{4\pi^2(c_0 \pm |c|/\sqrt{6})} = \frac{\sqrt{E_F}}{4\pi^2(c_0 \pm |c|/\sqrt{6})^{3/2}} \\ a_0 &= \frac{\hbar^2}{me^2} = \frac{2(c_0 \pm |c|/\sqrt{6})}{e^2} \\ q_\mathrm{TF}(\omega) &= \sqrt{8\pi e^2 N(0)/\varepsilon_c(\omega)} = \sqrt{\frac{e^2}{\pi\varepsilon_c(\omega)}\frac{\sqrt{E_F}}{(c_0 \pm |c|/\sqrt{6})^{3/2}}} \\ \mathrm{Ry} &= \frac{\hbar^2}{2ma_0^2} = \frac{me^4}{2\hbar^2} = \frac{e^4}{4(c_0 \pm |c|/\sqrt{6})}. \end{aligned} \tag{A12}$$

3. Parameter values

Yet another notation for the Hamiltonian density is used in Ref. [29],

$$\begin{aligned} \mathcal{H}_0(\mathbf{k}) = \alpha\mathbf{k}^2 + \beta\left(k_x^2J_x^2 + k_y^2J_y^2 + k_z^2J_z^2\right) + \gamma\sum_{\mu\neq\nu}k_\mu k_\nu J_\mu J_\nu \\ +\delta\sum_\mu k_\mu(J_{\mu+1}J_\mu J_{\mu+1} - J_{\mu+2}J_\mu J_{\mu+2}) - \mu, \end{aligned} \tag{A13}$$

which yields

$$\begin{cases} c_0 = \alpha + \frac{5}{4}\beta \\ c_1 = \sqrt{6}\gamma \\ c_2 = \sqrt{6}\beta \\ c_3 = \frac{\sqrt{3}}{2}\delta \end{cases}, \quad \text{i.e.,} \quad \begin{cases} \alpha = c_0 - \frac{5}{4\sqrt{6}}c_2 \\ \beta = \frac{c_2}{\sqrt{6}} \\ \gamma = \frac{c_1}{\sqrt{6}} \\ \alpha_4 = \frac{2c_3}{\sqrt{3}} \end{cases}. \tag{A14}$$

Plugging in the values given for YPtBi in the caption of Fig. 2 of Ref. [29], i.e.,

$$\begin{cases} \alpha = 20(a/\pi)^2\ \mathrm{eV} \\ \beta = -15(a/\pi)^2\ \mathrm{eV} \\ \gamma = -10(a/\pi)^2\ \mathrm{eV} \\ \delta = 0.1(a/\pi)^2\ \mathrm{eV} \end{cases} \text{so} \begin{cases} c_0 = 1.25(a/\pi)^2\ \mathrm{eV} \\ c_1 = -24.5(a/\pi)^2\ \mathrm{eV} \\ c_2 = -36.7(a/\pi)^2\ \mathrm{eV} \\ c_3 = 0.0866(a/\pi)^2\ \mathrm{eV} \end{cases}, \tag{A15}$$

and $\mu = -20$ meV, we obtain $|c_0/c_1| = 0.051 < 1/\sqrt{6}$ indeed, as well as, taking for a spherical approximation $c_3 = 0$ and $c_1 = c_2 = c \approx -30.6(a/\pi)^2$ eV, and the lattice constant $a = 6.65 \times 10^{-10}$ m,

$$\begin{aligned} m &= 7.5 \times 10^{-2} m_e = 6.83 \times 10^{-32}\,\mathrm{kg} \\ k_\mathrm{F} &= 2.0 \times 10^8\,\mathrm{m}^{-1} \\ n &= 1.33 \times 10^{23}\,\mathrm{m}^{-3} = 1.33 \times 10^{17}\,\mathrm{cm}^{-3} \\ N(0) &= 1.00 \times 10^{25}\,\mathrm{eV}^{-1}\,\mathrm{m}^{-3} \\ a_0 &= 13.3a_B = 7.01 \times 10^{-10}\,\mathrm{m} \\ q_\mathrm{TF} &= 4.3 \times 10^8\,\mathrm{m}^{-1} \\ \mathrm{Ry} &= 7.5 \times 10^{-2} \\ \mathrm{Ry}_0 &= 1.03\ \mathrm{eV} \\ E_\mathrm{F}/\mathrm{Ry} &= 1.9 \times 10^{-2} \\ q_\mathrm{TF}/k_\mathrm{F} &= 2.1 \\ \eta &= \frac{q_\mathrm{TF}^2}{2k_\mathrm{F}^2} = 2.3 \\ N(0)a_0^3 &= 3.4 \times 10^{-3}\ \mathrm{eV}^{-1} \\ N(0)/k_\mathrm{F}^3 &= 1.3\ \mathrm{eV}^{-1} \\ N(0)/q_\mathrm{TF}^3 &= 0.13\ \mathrm{eV}^{-1}, \end{aligned} \tag{A16}$$

where m_e is the electron mass, a_B is the Bohr radius, and Ry_0 is the Rydberg. Note that with these values [and in the spherical approximation taken with $c = (c_1 + c_2)/2$], we obtain a density $n = 1.33 \times 10^{17}$ cm^{-3}, smaller than the one reported experimentally, $n \sim 10^{18}$ cm^{-3}.

APPENDIX B: MATRICES AND PAIRINGS

In this Appendix and associated tables (Tables IV–VII), all matrices are orthonormalized according to the following scalar product:

$$(\mathcal{M}|\mathcal{N}) = \frac{1}{4\pi}\int d\hat{\mathbf{k}}\,\mathrm{Tr}[\mathcal{M}(\hat{\mathbf{k}})\mathcal{N}^\dagger(\hat{\mathbf{k}})], \tag{B1}$$

TABLE IV. Matrices M_S^α in spherical symmetry. The column "par." indicates whether S is even or odd (i.e., whether $M_S\gamma$ is antisymmetric or symmetric, respectively).

S	$\vec{M}_S$	par.
0	I_4	Even
2	$\frac{1}{\sqrt{2}}(-i\Gamma_3 - \Gamma_4, i\Gamma_1 + \Gamma_2, -\sqrt{2}\Gamma_5, i\Gamma_1 - \Gamma_2, i\Gamma_3 - \Gamma_4)$	Even
1	$\frac{\sqrt{2}}{\sqrt{5}}(J_x + iJ_y, -\sqrt{2}J_z, -J_x + iJ_y)$	Odd
3	$(M_3^3, M_3^2, M_3^1, M_3^0, M_3^{-1}, M_3^{-2}, M_3^{-3})$: see below	Odd

TABLE V. Odd parity pairing matrices $N_J^\alpha(\mathbf{k})$ with a single power of $\mathbf{k}$ in spherical symmetry.

J	S	$\vec{N}_J(\mathbf{k})$
0	1	$\frac{2}{\sqrt{5}}\mathbf{k}\cdot\mathbf{J}$
1	1	(N_1^1, N_1^0, N_1^{-1}): see below
2	1	$(N_{2^{(1)}}^2, N_{2^{(1)}}^1, N_{2^{(1)}}^0, N_{2^{(1)}}^{-1}, N_{2^{(1)}}^{-2})$: see below
2	3	$(N_{2^{(3)}}^2, N_{2^{(3)}}^1, N_{2^{(3)}}^0, N_{2^{(3)}}^{-1}, N_{2^{(3)}}^{-2})$: see below
3	3	$(N_3^3, N_3^2, N_3^1, N_3^0, N_3^{-1}, N_3^{-2}, N_3^{-3})$: see below
4	3	$(N_4^4, N_4^3, N_4^2, N_4^1, N_4^0, N_4^{-1}, N_4^{-2}, N_4^{-3}, N_4^{-4})$: see below

where $\mathcal{M}$ and $\mathcal{N}$ are 4×4 matrices that may or may not depend on $\hat{\mathbf{k}}$, and a matrix $\mathcal{M}$ is normalized if $(\mathcal{M}|\mathcal{M}) = 4$.

For convenience, we define $\mathcal{J} = \frac{-41}{6\sqrt{5}}\mathbf{J} + \frac{2\sqrt{5}}{3}(J_x^3, J_y^3, J_z^3)$. Note that $(\mathcal{J}^\mu|J^\nu) = 0\ \forall \mu,\nu$.

1. Spherical symmetry

$$
\begin{aligned}
M_3^3 &= \frac{1}{2}(-i\Gamma_{13} - \Gamma_{14} - \Gamma_{23} + i\Gamma_{24})\\
M_3^2 &= \frac{1}{\sqrt{2}}(-\Gamma_{35} + i\Gamma_{45})\\
M_3^1 &= \frac{\sqrt{3}}{2\sqrt{5}}\left(-i\Gamma_{13} - \Gamma_{14} + \frac{2}{\sqrt{3}}\Gamma_{15} + \Gamma_{23} - i\Gamma_{24} - \frac{2i}{\sqrt{3}}\Gamma_{25}\right)\\
M_3^0 &= \frac{1}{\sqrt{5}}(2\Gamma_{12} - \Gamma_{34}) \quad M_3^{-m} = \left(M_3^m\right)^\dagger\ \forall\, m,
\end{aligned}
\tag{B2}
$$

$\mathbf{k}$ transforms as $L = 1$ for SO(3) operations

$$
\begin{aligned}
N_1^1(\mathbf{k}) &= \frac{\sqrt{3}}{\sqrt{5}}[-k_z(J_x + iJ_y) + (k_x + ik_y)J_z]\\
N_1^0(\mathbf{k}) &= i\frac{\sqrt{6}}{\sqrt{5}}(k_yJ_x - k_xJ_y),\\
N_{2^{(1)}}^2(\mathbf{k}) &= \frac{\sqrt{3}}{\sqrt{5}}[(k_x + ik_y)(J_x + iJ_y)]\\
N_{2^{(1)}}^1(\mathbf{k}) &= \frac{\sqrt{3}}{\sqrt{5}}[-k_z(J_x + iJ_y) - (k_x + ik_y)J_z]
\end{aligned}
\tag{B3}
$$

$$
\begin{aligned}
N_{2^{(1)}}^0(\mathbf{k}) &= i\frac{\sqrt{2}}{\sqrt{5}}(-k_xJ_x - k_yJ_y + 2k_zJ_z),\\
N_{2^{(3)}}^2(\mathbf{k}) &= \frac{\sqrt{3}}{\sqrt{5}}[-k_z(J_x + iJ_y) + (k_x + ik_y)J_z]\\
N_{2^{(3)}}^1(\mathbf{k}) &= \frac{\sqrt{3}}{\sqrt{5}}[-k_z(J_x + iJ_y) + (k_x + ik_y)J_z]\\
N_{2^{(3)}}^0(\mathbf{k}) &= i\frac{\sqrt{6}}{\sqrt{5}}(k_yJ_x - k_xJ_y),
\end{aligned}
\tag{B4}
$$

TABLE VI. Matrices $\vec{M}_R$ in cubic symmetry with inversion O_h, and in tetrahedral symmetry T_d (where one simply reads the representation labels with the g index dropped). The parity column "par." indicates whether $M_R\gamma$ is symmetric (odd) or antisymmetric (even).

R	$\vec{M}_R$	par.	$R(T_d)$
A_{1g}	I_4	Even	A_1
E_g	(Γ_4, Γ_5)	Even	E
T_{2g}	$(\Gamma_1, \Gamma_2, \Gamma_3)$	Even	T_2
T_{1g}	$\frac{2}{\sqrt{5}}(J_x, J_y, J_z)$	Odd	T_1
A_{2g}	$\frac{2}{\sqrt{3}}(J_xJ_yJ_z + J_zJ_yJ_x) = -\Gamma_{45}$	Odd	A_2
T_{1g}	$\frac{-41}{6\sqrt{5}}\mathbf{J} + \frac{2\sqrt{5}}{3}(J_x^3, J_y^3, J_z^3)$	Odd	T_1
T_{2g}	$\frac{-1}{\sqrt{3}}(T_x, T_y, T_z)$	Odd	T_2

$$
\begin{aligned}
N_3^3(\mathbf{k}) &= \frac{1}{2}Y_{11}M_3^2 - \frac{\sqrt{3}}{2}Y_{10}M_3^3\\
N_3^2(\mathbf{k}) &= \sqrt{\frac{5}{12}}Y_{11}M_3^1 - \sqrt{\frac{1}{3}}Y_{10}M_3^2 - \frac{1}{2}Y_{1-1}M_3^3\\
N_3^1(\mathbf{k}) &= \frac{1}{\sqrt{2}}Y_{11}M_3^0 - \frac{1}{2\sqrt{3}}Y_{10}M_3^1 - \sqrt{\frac{5}{12}}Y_{1-1}M_3^2\\
N_3^0(\mathbf{k}) &= \sqrt{\frac{1}{2}}Y_{11}M_3^{-1} - \sqrt{\frac{1}{2}}Y_{1-1}M_3^1,
\end{aligned}
\tag{B6}
$$

$$
\begin{aligned}
N_4^4(\mathbf{k}) &= Y_{11}M_3^3\\
N_4^3(\mathbf{k}) &= \frac{\sqrt{3}}{2}Y_{11}M_3^3 + \frac{1}{2}Y_{10}M_3^3\\
N_4^2(\mathbf{k}) &= \sqrt{\frac{15}{28}}Y_{11}M_3^1 - \sqrt{\frac{3}{7}}Y_{10}M_3^2 + \frac{1}{2\sqrt{7}}Y_{1-1}M_3^3\\
N_4^1(\mathbf{k}) &= \sqrt{\frac{5}{14}}Y_{11}M_3^0 + \sqrt{\frac{15}{28}}Y_{10}M_3^1 + \sqrt{\frac{5}{28}}Y_{1-1}M_3^2\\
N_4^0(\mathbf{k}) &= \sqrt{\frac{3}{14}}Y_{11}M_3^{-1} + \sqrt{\frac{4}{7}}Y_{10}M_3^0 + \sqrt{\frac{3}{14}}Y_{1-1}M_3^1,
\end{aligned}
\tag{B7}
$$

where the $Y_{lm}(\hat{\mathbf{k}})$ are the usual spherical harmonics, normalized following $\frac{1}{4\pi}\int d\hat{\mathbf{k}}Y_{lm}^*(\hat{\mathbf{k}})Y_{lm}(\hat{\mathbf{k}}) = 1$ [and we have switched in Eqs. (B6) and (B7) from the k^μ to the spherical harmonic notation for compactness).

2. Cubic symmetry O_h

In which "form" we write down the matrices (Γ_a or J^μ) in the tables and equations is entirely determined by the simplest form.

$\mathbf{k}$ transforms under the T_{1u} representation of O_h.

3. Tetrahedral symmetry T_d

In tetrahedral symmetry, $\mathbf{k}$ transforms according to T_2 (instead of T_{1u} in cubic symmetry) so that one needs only modify the symmetric pairing functions labels $A_{1u}\to A_2$, $A_{2u}\to A_1$, $E_u\to E$, $T_{1u}\to T_2$, and $T_{2u}\to T_1$ (see the rightmost column of Table VII). The basis matrices M_R are unchanged except for the drop of the g subscript.

APPENDIX C: FIERZ IDENTITIES

Fierz identities [36,46,47] are reordering relations for four-fermion interactions: if A and B are two $n\times n$ matrices, and ψ_i

TABLE VII. Odd parity pairing matrices $\vec{N}_{R'}(\mathbf{k})$ with a single power of $\mathbf{k}$ in cubic symmetry with inversion O_h, and in tetrahedral symmetry T_d (read the representation labels on the right-hand side).

R'	$\vec{N}_{R'}(\mathbf{k})$	$R'(T_d)$
A_{1u}	$\frac{2}{\sqrt{5}}\mathbf{k}\cdot\mathbf{J}$	A_2
T_{1u}	$\frac{\sqrt{6}}{\sqrt{5}}\mathbf{J}\times\mathbf{k}$	T_2
E_u	$\frac{\sqrt{2}}{\sqrt{5}}[-J_xk_x-J_yk_y+2J_zk_z,\sqrt{3}(J_xk_x-J_yk_y)]$	E
T_{2u}	$\frac{\sqrt{6}}{\sqrt{5}}(J_yk_z+J_zk_y,J_xk_z+J_zk_x,J_xk_y+J_yk_x)$	T_1
T_{2u}	$-2\Gamma_{45}\mathbf{k}$	T_1
A_{1u}	$\mathcal{J}\cdot\mathbf{k}$	A_2
E_u	$\frac{1}{\sqrt{2}}[-k_x\mathcal{J}_x-k_y\mathcal{J}_y+2k_z\mathcal{J}_z,\sqrt{3}(k_x\mathcal{J}_x-k_y\mathcal{J}_y)]$	E
T_{1u}	$\frac{\sqrt{3}}{\sqrt{2}}\mathcal{J}\times\mathbf{k}$	T_2
T_{2u}	$\frac{\sqrt{3}}{\sqrt{2}}(\mathcal{J}_yk_z+\mathcal{J}_zk_y,\mathcal{J}_xk_z+\mathcal{J}_zk_x,\mathcal{J}_xk_y+\mathcal{J}_yk_x)$	T_1
A_{2u}	$\frac{1}{\sqrt{3}}\mathbf{T}\cdot\mathbf{k}$	A_1
E_u	$\frac{1}{\sqrt{6}}[T_xk_x+T_yk_y-2T_zk_z,\sqrt{3}(T_xk_x-T_yk_y)]$	E
T_{1u}	$\frac{1}{\sqrt{2}}(T_yk_z+T_zk_y,T_xk_z+T_zk_x,T_xk_y+T_yk_x)$	T_2
T_{2u}	$\frac{1}{\sqrt{2}}\mathbf{T}\times\mathbf{k}$	T_1

n-component fermion fields, there exist matrices A',B',A'',B'' such that

$$(\psi_1^\dagger A\psi_2)(\psi_3^\dagger B\psi_4)=(\psi_1^\dagger A'\psi_4)(\psi_3^\dagger B'\psi_2) \tag{C1}$$

$$=(\psi_1^\dagger A''\psi_3^\dagger)(\psi_4 B''\psi_2) \tag{C2}$$

$$=-(\psi_1^\dagger A''\psi_3^\dagger)(\psi_2 B''^T\psi_4), \tag{C3}$$

by virtue of the simple anticommutation relations between field operators. Ultimately these identities correspond to a change of basis for tensor products. Here we do not derive Fierz identities in great generality, but rather focus on special cases useful for our purposes.

1. Derivation

Let $\{Q_a\}_{a=1,\dots,n^2}$ be an orthonormal basis of the Hilbert space of $n\times n$ matrices. (In particular $\mathrm{Tr}[Q_aQ_b^\dagger]=n\,\delta_{ab}$.) Then, any matrix A in that space can be expanded following

$$A=\sum_a A^aQ_a,\qquad \text{where}\qquad A^a=\frac{1}{n}\mathrm{Tr}[A^\dagger Q_a]. \tag{C4}$$

A set of basis matrices can be chosen as basis matrices of the irreducible representations of the symmetry group forming the Hilbert space. We call such a set $\{\vec{W}_R\}_R$, where the dimension of each vector $\vec{W}_R$ is that of the dimension of R. We take $\mathrm{Tr}[W_R^iW_{R'}^{j\,\dagger}]=n\,\delta_{ij}\,\delta_{RR'}$.

a. Particle-hole relation

Elements of the trivial representations can be formed out of every representation as follows:

$$\vec{W}_R\cdot\vec{W}_R^\dagger\equiv\sum_{i=1}^{\dim R}W_R^i\otimes W_R^i. \tag{C5}$$

For a given representation R_o, we wish to find the coefficients $f(R_o,R)$ such that

$$\big[\vec{W}_{R_o}\big]_{\alpha\beta}\cdot[\vec{W}_{R_o}^\dagger]_{\mu\nu}=\sum_R f(R_o,R)[\vec{W}_R]_{\alpha\nu}\cdot[\vec{W}_R^\dagger]_{\mu\beta}. \tag{C6}$$

Multiplying Eq. (C6) by ${W_{R_1,\lambda\alpha}^i}^\dagger W_{R_1,\rho\mu}^i$ and summing over α and μ, we find

$$\sum_{j=1}^{\dim R_o}\big[{W_{R_1}^i}^\dagger W_{R_o}^j\big]_{\lambda\beta}\big[W_{R_1}^i\,{W_{R_o}^j}^\dagger\big]_{\rho\nu}$$

$$=\sum_R f(R_o,R)\sum_{j=1}^{\dim R}\big[{W_{R_1}^i}^\dagger W_R^j\big]_{\lambda\nu}\big[W_{R_1}^i\,W_R^{j\dagger}\big]_{\rho\beta}. \tag{C7}$$

Now taking $\lambda=\nu$ and $\rho=\beta$ and summing over λ,ρ, we find

$$f(R_o,R_1)=\frac{1}{n^2}\sum_{j=1}^{\dim R_o}\mathrm{Tr}\big[{W_{R_1}^i}^\dagger W_{R_o}^jW_{R_1}^i\,{W_{R_o}^j}^\dagger\big] \tag{C8}$$

for any $i=1,\dots,\dim R_o$.

b. Particle-particle relation

Similarly, we wish to find the coefficients $g(R_o,R)$ such that

$$\big[\vec{W}_{R_o}\big]_{\alpha\beta}\cdot\big[\vec{W}_{R_o}^\dagger\big]_{\mu\nu}=\sum_R g(R_o,R)[\vec{W}_R\Lambda]_{\alpha\mu}\cdot[\Lambda^T\vec{W}_R^\dagger]_{\nu\beta}, \tag{C9}$$

where here we have $\overline{R}=R\Lambda$, with $\Lambda^T=-\Lambda$, $\Lambda^T\Lambda=\Lambda\Lambda^T=\mathrm{Id}_n$. Here we multiply Eq. (C9) by $[\Lambda^T{W_{R_1}^i}^\dagger]_{\lambda\alpha}[W_{R_1}^i\Lambda]_{\rho\nu}$ and sum over α,ν:

$$\sum_{j=1}^{\dim R_o}\big[\Lambda^T{W_{R_1}^i}^\dagger W_{R_o}^j\big]_{\lambda\beta}\big[W_{R_1}^i\Lambda\,W_{R_o}^{j\,*}\big]_{\rho\mu}$$

$$=\sum_R g(R_o,R)\sum_{j=1}^{\dim R}\big[\Lambda^T{W_{R_1}^i}^\dagger W_R^j\Lambda\big]_{\lambda\mu}[W_{R_1}^iW_R^{j\dagger}]_{\rho\beta}, \tag{C10}$$

and we obtain, setting $\lambda=\mu$ and $\rho=\beta$ and summing over λ,ρ:

$$g(R_o,R_1)=\frac{\eta_{R_o}}{n^2}\sum_{j=1}^{\dim R_o}\mathrm{Tr}\big[{W_{R_1}^i}^\dagger W_{R_o}^jW_{R_1}^i\,{W_{R_o}^j}^\dagger\big]$$

$$=\eta_{R_o}f(R_o,R_1), \tag{C11}$$

where $\eta_R=\pm1$ is such that $\Lambda W_R^{j\,*}\Lambda^T=\eta_RW_R^{j\dagger}$.

APPENDIX D: ELIASHBERG THEORY

1. Details of calculations from the main text

a. Spherical (or cubic) harmonic decomposition

The components of the interaction $V_{0,1}$ defined in Eq. (15) are

$$V_0(|\mathbf{k}|,|\mathbf{k}'|;\omega-\omega')=\frac{1}{4\pi}\int d\hat{\mathbf{k}}d\hat{\mathbf{k}}'V(\mathbf{k}-\mathbf{k}',\omega-\omega'),$$

$$V_1(|\mathbf{k}|,|\mathbf{k}'|;\omega-\omega')=\frac{1}{4\pi}\int d\hat{\mathbf{k}}d\hat{\mathbf{k}}'(\hat{\mathbf{k}}\cdot\hat{\mathbf{k}}')V(\mathbf{k}-\mathbf{k}',\omega-\omega'), \tag{D1}$$

where $\int d\hat{\mathbf{k}} = \int_0^{\pi} d\theta \sin\theta \int_0^{2\pi} d\phi$.

b. Projected representation mixing

When several copies of a representation appear, one must solve for a mixture of matrices belonging to each copy. In the $J = 2$ case, defining

$$\Sigma_A(k) = \Delta(\omega) \sum_{i=1,2} \phi_i n^{\alpha}_{2,i}(\hat{\mathbf{k}}), \tag{D2}$$

one must now solve

$$\sum_{i,i'} n^{\alpha}_{J,i}(\hat{\mathbf{k}}) \left[\Delta(\omega)\delta_{ii'} + \frac{\pi}{\beta_c} \mathcal{L}_J(\omega) A^{ii'}_J \right] \phi_{i'} = 0, \tag{D3}$$

where

$$\mathcal{L}_j(\omega) = \sum_{\omega'} \frac{\Delta(\omega')}{|\omega'|} f_J(\omega - \omega'). \tag{D4}$$

This is equivalent to solving

$$\mathbf{A}_J \left[\Delta(\omega) + \frac{\pi}{\beta_c} \mathcal{L}_J(\omega) \mathbf{A}_J \right] = \mathbf{0}, \tag{D5}$$

where $\mathbf{A}_J = (A^{ii'}_J)_{ii'}$ (the fifth row of Table III), and hence a set of solutions is given by solving for the eigenvalues and eigenvectors of $\mathbf{A}_J$.

The eigenvalues and eigenvectors of $A_{J=2,ii'}$ of Table III lead to the following pairing strengths and matrices. For the 3/2 bands:

$$\begin{aligned} \tilde{A} = 27/70, \quad \tilde{n}_{J=2,1}, &= \frac{1}{\sqrt{15}}(-\sqrt{14} n_{J=2,S=1} + n_{J=2,S=3}) \\ \tilde{A} = 0, \quad \tilde{n}_{J=2,2} &= \frac{1}{\sqrt{15}}(n_{J=2,S=1} + \sqrt{14} n_{J=2,S=3}), \end{aligned} \tag{D6}$$

and for the 1/2 bands:

$$\begin{aligned} \tilde{A} = \frac{55+\sqrt{2689}}{140}, \quad \tilde{n}_{J=2,1} &= \sqrt{\frac{1}{2} - \frac{79}{10\sqrt{2689}}} n_{J=2,S=1} \\ &\quad + \sqrt{\frac{1}{2} + \frac{79}{10\sqrt{2689}}} n_{J=2,S=3} \\ \tilde{A} = \frac{55-\sqrt{2689}}{140}, \quad \tilde{n}_{J=2,2} &= -\sqrt{\frac{1}{2} + \frac{79}{10\sqrt{2689}}} n_{J=2,S=1} \\ &\quad + \sqrt{\frac{1}{2} - \frac{79}{10\sqrt{2689}}} n_{J=2,S=3}. \end{aligned} \tag{D7}$$

[1] Y. S. Hor, A. J. Williams, J. G. Checkelsky, P. Roushan, J. Seo, Q. Xu, H. W. Zandbergen, A. Yazdani, N. P. Ong, and R. J. Cava, Superconductivity in $Cu_xBi_2Se_3$ and its Implications for Pairing in the Undoped Topological Insulator, Phys. Rev. Lett. **104**, 057001 (2010).

[2] I. A. Chernik and S. N. Lykov, Sov. Phys. Solid State **23**, 817 (1981).

[3] O. Prakash, A. Kumar, A. Thamizhavel, and S. Ramakrishnan, Evidence for bulk superconductivity in pure bismuth single crystals at ambient pressure, Science **355**, 52 (2016).

[4] Y. Nakajima, R. Hu, K. Kirshenbaum, A. Hughes, P. Syers, X. Wang, K. Wang, R. Wang, S. R. Saha, D. Pratt, J. W. Lynn, and J. Paglione, Topological RPdBi half-Heusler semimetals: A new family of noncentrosymmetric magnetic superconductors, Sci. Adv. **1**, e1500242 (2015).

[5] J. F. Schooley, W. R. Hosler, and M. L. Cohen, Superconductivity in Semiconducting $SrTiO_3$, Phys. Rev. Lett. **12**, 474 (1964).

[6] J. M. Luttinger, Quantum theory of cyclotron resonance in semiconductors: General theory, Phys. Rev. **102**, 1030 (1956).

[7] M. Cardona and D. L. Greenaway, Fundamental reflectivity and band structure of ZnTe, CdTe, and HgTe, Phys. Rev. **131**, 98 (1963).

[8] S. Chadov, X. Qi, J. Kübler, G. H. Fecher, C. Felser, and S. C. Zhang, Tunable multifunctional topological insulators in ternary Heusler compounds, Nat. Mater. **9**, 541 (2010).

[9] B.-J. Yang and Y. B. Kim, Topological insulators and metal-insulator transition in the pyrochlore iridates, Phys. Rev. B **82**, 085111 (2010).

[10] E.-G. Moon, C. Xu, Y. B. Kim, and L. Balents, Non-Fermi-Liquid and Topological States with Strong Spin-Orbit Coupling, Phys. Rev. Lett. **111**, 206401 (2013).

[11] L. Savary, E.-G. Moon, and L. Balents, New Type of Quantum Criticality in the Pyrochlore Iridates, Phys. Rev. X **4**, 041027 (2014).

[12] W. Witczak-Krempa and Y. B. Kim, Topological and magnetic phases of interacting electrons in the pyrochlore iridates, Phys. Rev. B **85**, 045124 (2012).

[13] J. M. Murray, O. Vafek, and L. Balents, Incommensurate spin density wave at a ferromagnetic quantum critical point in a three-dimensional parabolic semimetal, Phys. Rev. B **92**, 035137 (2015).

[14] B.-J. Yang and N. Nagaosa, Emergent Topological Phenomena in Thin Films of Pyrochlore Iridates, Phys. Rev. Lett. **112**, 246402 (2014).

[15] K. Matsuhira, M. Wakeshima, Y. Hinatsu, and S. Takagi, Metalinsulator transitions in pyrochlore oxides $Ln_2Ir_2O_7$, J. Phys. Soc. Jpn. **80**, 094701 (2011).

[16] W. Witczak-Krempa, G. Chen, Y.-B. Kim, and L. Balents, Correlated quantum phenomena in the strong spin-orbit regime, Annu. Rev. Condens. Matter Phys. **5**, 57 (2014).

[17] P. G. Pagliuso, C. Rettori, M. E. Torelli, G. B. Martins, Z. Fisk, J. L. Sarrao, M. F. Hundley, and S. B. Oseroff, Crystal-field study in rare-earth-doped semiconducting YBiPt, Phys. Rev. B **60**, 4176 (1999).

[18] G. Goll, M. Marz, A. Hamann, T. Tomanic, K. Grube, T. Yoshino, and T. Takabatake, Thermodynamic and transport properties of the non-centrosymmetric superconductor LaBiPt, Physica B (Amsterdam) **403**, 1065 (2008).

[19] N. P Butch, P Syers, K. Kirshenbaum, A. P Hope, and J. Paglione, Superconductivity in the topological semimetal YPtBi, Phys. Rev. B **84**, 220504 (2011).

[20] Y. Pan, A. M. Nikitin, T. V. Bay, Y. K. Huang, C. Paulsen, B. H. Yan, and A. de Visser, Superconductivity and magnetic order

in the noncentrosymmetric half-Heusler compound ErPdBi, Europhys. Lett. **104**, 27001 (2013).

[21] F. F. Tafti, T. Fujii, A. Juneau-Fecteau, S. René de Cotret, N. Doiron-Leyraud, A. Asamitsu, and L. Taillefer, Superconductivity in the noncentrosymmetric half-Heusler compound LuPtBi: A candidate for topological superconductivity, Phys. Rev. B **87**, 184504 (2013).

[22] G. Xu, W. Wang, X. Zhang, Y. Du, E. Liu, S. Wang, G. Wu, Z. Liu, and X. X. Zhang, Weak antilocalization effect and noncentrosymmetric superconductivity in a topologically nontrivial semimetal LuPdBi, Sci. Rep. **4**, 5709 (2014).

[23] A. M. Nikitin, Y. Pan, X. Mao, R. Jehee, G. K. Araizi, Y. K. Huang, C. Paulsen, S. C. Wu, B. H. Yan, and A. de Visser, Magnetic and superconducting phase diagram of the half-Heusler topological semimetal HoPdBi, J. Phys.: Condens. Matter **27**, 275701 (2015).

[24] Z. K. Liu, L. X. Yang, S. C. Wu, C. Shekhar, J. Jiang, H. F. Yang, Y. Zhang, S. K. Mo, Z. Hussain, B. Yan, C. Felser, and Y. L. Chen, Observation of unusual topological surface states in half-Heusler compounds LnPtBi (Ln = Lu, Y), Nat. Commun. **7**, 12924 (2016).

[25] X. Zhang, Z. Hou, Y. Wang, G. Xu, C. Shi, E. Liu, X. Xi, W. Wang, G. Wu, and X.-x. Zhang, NMR evidence for the topologically nontrivial nature in a family of half-Heusler compounds, Sci. Rep. **6**, 23172 (2016).

[26] H. Kim, K. Wang, Y. Nakajima, R. Hu, S. Ziemak, P. Syers, L. Wang, H. Hodovanets, J. D. Denlinger, P. M. R. Brydon, D. F. Agterberg, M. A. Tanatar, R. Prozorov, and J. Paglione, Beyond triplet: Unconventional superconductivity in a spin-3/2 topological semimetal, arXiv:1603.03375.

[27] Though in Ref. [8] it is argued that the Fermi energy in (Sm,Eu,Gd,Tb,Dy,Y)PdBi compounds might instead be close to another set, Γ_6.

[28] M. Meinert, Unconventional Superconductivity in YPtBi and Related Topological Semimetals, Phys. Rev. Lett. **116**, 137001 (2016).

[29] P. M. R. Brydon, L. Wang, M. Weinert, and D. F. Agterberg, Pairing of $j = 3/2$ Fermions in Half-Heusler Superconductors, Phys. Rev. Lett. **116**, 177001 (2016).

[30] J. Ruhman and P. A. Lee, Superconductivity at very low density: The case of strontium titanate, Phys. Rev. B **94**, 224515 (2016).

[31] This problem will be addressed in future work.

[32] L. V. Gurevich, A. I. Larkin, and Y. A. Firsov, On the possibility of superconductivity in semiconductors, Sov. Phys. Solid State **4**, 131 (1962).

[33] H. Fröhlich, Electrons in lattice fields, Adv. Phys. **3**, 325 (1954).

[34] C. Verdi and F. Giustino, Fröhlich Electron-Phonon Vertex from First Principles, Phys. Rev. Lett. **115**, 176401 (2015).

[35] G. Dresselhaus, Spin-orbit coupling effects in zinc blende structures, Phys. Rev. **100**, 580 (1955).

[36] I. Boettcher and I. F. Herbut, Superconducting quantum criticality in three-dimensional Luttinger semimetals, Phys. Rev. B **93**, 205138 (2016).

[37] C. Fang, B. A. Bernevig, and M. J. Gilbert, Tri-Dirac surface modes in topological superconductors, Phys. Rev. B **91**, 165421 (2015).

[38] W. Yang, Y. Li, and C. Wu, Topological Septet Pairing with Spin-$\frac{3}{2}$ Fermions: High-Partial-Wave Channel Counterpart of the ^{3}He-B Phase, Phys. Rev. Lett. **117**, 075301 (2016).

[39] J. R. Schrieffer, *Theory of Superconductivity* (Pennsylvania University Press, Philadelphia, 1963).

[40] The physical reason for this is that the angular momentum difference between a pair of quasiparticles at $\mathbf{k}$ and $-\mathbf{k}$ in the same band 3/2 and σ is three units of angular momentum. Scattering between different momentum states of this type requires a higher angular momentum.

[41] D. F. Agterberg, P. M. R. Brydon, and C. Timm, Bogoliubov Fermi Surfaces in Superconductors with Broken Time-Reversal Symmetry, Phys. Rev. Lett. **118**, 127001 (2017).

[42] C. Timm, A. P. Schnyder, D. F. Agterberg, and P. M. R. Brydon, Inflated nodes and surface states in superconducting half-Heusler compounds, Phys. Rev. B **96**, 094526 (2017).

[43] I. Boettcher and I. F. Herbut, Unconventional superconductivity in Luttinger semimetals: Theory of complex tensor order and emergence of the uniaxial nematic state, arXiv:1707.03444.

[44] Y. Wang and L. Fu, Topological Phase Transitions in Multicomponent Superconductors, Phys. Rev. Lett. **119**, 187003 (2017).

[45] S. Murakami, N. Nagaosa, and S.-C. Zhang, SU(2) non-Abelian holonomy and dissipationless spin current in semiconductors, Phys. Rev. B **69**, 235206 (2004).

[46] M. Fierz, Zur fermischen theorie des β-Zerfalls, Z. Phys. **104**, 553 (1937).

[47] O. Vafek, J. M. Murray, and V. Cvetkovic, Superconductivity on the Brink of Spin-Charge Order in a Doped Honeycomb Bilayer, Phys. Rev. Lett. **112**, 147002 (2014).